

# Twin Tests Book of Reference

## Twin Test 2: Wake interactions of a cluster of turbines and wake steering techniques

Lead Beneficiary: NTUA  
Dissemination Level: Public

Authors: V. Pappa, F. Muehle, S. Tamaro, F.  
Campagnolo, C. Bottasso, B. Dsouza, A.  
Siacchitano, P. Chasapogiannis,  
M. Manolesos,

# WP4

---

## Widening of technical capacity and competence

**Deliverable 4.1**

TWEET-IE / Twin Wind tunnels for Energy and the  
EnvironmentT - Innovations and Excellence  
HORIZON-WIDERA-2021-ACCESS-03-01 / PR# 101079125



Co-funded by  
the European Union

## Executive Summary

The present chapter of the book of references refers to the first twin test of the TWEET-IE project, carried out in the wind tunnels of the Technical University of Munich (TUM) and the National Technical University of Athens (NTUA). For the tests at NTUA state of the art Volumetric Particle Tracking Velocimetry (PTV) from the Technical University of Delft was used.

The investigation focuses on the interaction between two turbine models and more specifically on two wake control methods, the Helix and Wake Steering by yaw misalignment. Results include power measurements from the two models (both tunnels), hot wire anemometry measurements (NTUA) and Volumetric Particle Tracking Velocimetry (NTUA). There is very good agreement between the results from the two wind tunnels both for the uncontrolled case and when the two wake control methods are employed.

## History and Changes

Ver	Date	Description	Contributors
1.0	25/07/2024	Report	NTUA, TUM, TUD

# Contents

<b>EXECUTIVE SUMMARY</b>	<b>2</b>
<b>HISTORY AND CHANGES</b>	<b>3</b>
<b>CONTENTS</b>	<b>4</b>
<b>LIST OF FIGURES</b>	<b>5</b>
<b>LIST OF TABLES</b>	<b>ERROR! BOOKMARK NOT DEFINED.</b>
<b>1 INTRODUCTION</b>	<b>7</b>
<b>2 TUM - EQUIPMENT AND METHODS. TRAINING AND DOCUMENTATION</b>	<b>8</b>
2.1 TUM FACILITY AND EQUIPMENT	8
2.1.1 <i>The wind tunnel at TUM</i>	8
2.1.2 <i>Equipment</i>	9
2.1.3 <i>Inflow velocity and turbulence intensity profiles</i>	9
2.1.4 <i>Wind Turbine Models</i>	10
2.1.5 <i>Wind Turbine model calibration procedure</i>	11
2.1.5.1 Task 1: Set-up	12
2.1.5.2 Task 2: Blade calibration	12
2.1.5.3 Task 3: Shaft calibration	14
2.1.5.4 Task 4: Tower calibration	17
<b>3 NTUA - EQUIPMENT AND METHODS. APPLIED KNOWLEDGE.</b>	<b>20</b>
3.1 THE NTUA WIND TUNNEL SET UP	20
3.2 INFLOW	20
3.3 HOT WIRE ANEMOMETRY	21
3.4 PARTICLE TRACKING VELOCIMETRY	22
3.5 WAKE CONTROL TECHNIQUES	27
<b>4 TWIN TEST 2: WAKE INTERACTIONS OF A CLUSTER OF TURBINES AND WAKE STEERING TECHNIQUES</b>	<b>28</b>
4.1 TUM RESULTS	28
4.1.1 <i>Pressure variation along the test section</i>	28
4.1.2 <i>Inflow velocity and turbulence intensity profiles</i>	28
4.1.3 <i>Wind Turbine Performance</i>	29
4.2 NTUA RESULTS	31
4.2.1 <i>Inflow</i>	31
4.2.2 <i>Helix, Low Turbulence – Comparison with TUM results</i>	32
4.2.3 <i>Helix, High Turbulence – Comparison with TUM results</i>	34
4.2.4 <i>Combination of Helix with Static Yaw – Low Turbulence</i>	35
4.2.5 <i>Combination of Helix with Static Yaw – High Turbulence</i>	37
<b>5 REFERENCES</b>	<b>40</b>

## List of figures

<b>Figure 1.</b> Sketch of the wind tunnel test section with the positioning of the pressure taps in the centre of the wind tunnel ceiling, the location of the pitot tube and the locations of the upstream and downstream wind turbine models. ....	8
<b>Figure 2.</b> Streamwise (x, m) and vertical (z, m) coordinates of the pressure taps at different positions, along the centre of the wind tunnel ceiling; b). ....	9
<b>Figure 3.</b> Fast-response five-hole probe equipped with piezo-resistive sensors, adapted from [2]. ...	9
<b>Figure 4.</b> The G1 wind turbine with highlighted components .....	10
<b>Figure 5.</b> Chord and twist distribution for the G1 wind turbine model .....	11
Figure 6. Orientation of the turbine parts.....	11
Figure 7. Tools needed for calibration.....	12
<b>Figure 8.</b> Binary numbering of nodes on EPOS.....	13
<b>Figure 9.</b> Detaching of the generator and torquemeter .....	15
<b>Figure 10.</b> Sign of angles on inclinometer .....	15
<b>Figure 11.</b> Positions on the weight plate .....	16
<b>Figure 12.</b> Position of inclinometer for tower calibration.....	18
<b>Figure 13.</b> Sketch of the NTUA wind tunnel test section with the location of the pitot tube and the locations of the upstream and downstream wind turbine models, when high turbulence intensity (screen and passive grid) is applied (not to scale). ....	20
<b>Figure 14.</b> Upstream view of the test section with the passive grid installed. ....	21
<b>Figure 15.</b> Single wire sensor used for the inflow measurements. ....	22
<b>Figure 16.</b> Pressure drop along the ceiling of the test section (in the streamwise direction): a) without wind turbine models in the wind tunnel test section and b) with both wind turbine models installed: the upstream turbine model operates at $\omega_{upstream} = 850$ rpm while the downstream turbine model operates at $\omega_{downstream} = 574$ rpm.....	28
<b>Figure 17.</b> Vertical inflow profiles of a) streamwise velocity U (m/s) (error bars: standard deviation of streamwise velocity); and b) turbulence intensity, $TI_u$ (%) in the empty wind tunnel test section, at the positions of the two wind turbine models. ....	29
<b>Figure 18.</b> a) Streamwise velocity, u (m/s) and b) Turbulence intensity, $TI_u$ (%) variation along the spanwise direction in the empty wind tunnel test section, at the positions of the two wind turbine models. ....	29
<b>Figure 19.</b> a) Power, $P$ ; b) power coefficient, $CP$ ; and c) thrust coefficient $CT$ variation with tip speed ratio, $\lambda$ , when each of the turbine models is placed independently in the wind tunnel test section. ....	30
<b>Figure 20.</b> a) Power, $P$ ; b) power coefficient, $CP$ ; and c) thrust coefficient $CT$ variation with upstream turbine tip speed ratio, $\lambda_{upstream}$ , when both wind turbines are placed in the wind tunnel test section. The upstream wind turbine model rotates at variable rotational speed while the downstream wind turbine rotates at constant rotor speed (574 rpm, $\lambda_{downstream} = 5.86$ ). ....	30
<b>Figure 21.</b> a) Power, $P$ ; b) power coefficient, $CP$ ; and c) thrust coefficient $CT$ variation with downstream turbine tip speed ratio, $\lambda_{downstream}$ , when both wind turbines are placed in the wind tunnel test section. The upstream wind turbine model rotates at constant rotational speed (850 rpm, $\lambda_{upstream} = 8.53$ ) while the downstream wind turbine rotates at variable rotor speed. ....	30
<b>Figure 22.</b> Low turbulence case. Inflow velocity and turbulence intensity profiles at the location of the wind turbine rotor at locations A, B and C as indicated in <i>Figure 13</i> . ....	31

<b>Figure 23.</b> High turbulence case. Inflow velocity and turbulence intensity profiles at the location of the wind turbine rotor at locations A, B and C as indicated in <i>Figure 13</i> .	32
<b>Figure 24.</b> Horizontal inflow velocity and turbulence intensity profiles at hub height between positions B and C, as indicated in <i>Figure 13</i> .	32
<b>Figure 25.</b> Relative power performance of the two turbines with respect to the no control case. Comparison between measurements at TUM and at NTUA.	33
<b>Figure 26.</b> Relative power performance of the upstream turbine with respect to the no control case. Comparison between measurements at TUM and at NTUA.	33
<b>Figure 27.</b> Relative power performance of the downstream turbine with respect to the no control case. Comparison between measurements at TUM and at NTUA.	34
<b>Figure 28.</b> Relative power performance of the two turbines with respect to the no control case. NTUA: High Turbulence inflow, TUM: ABL inflow. Comparison between measurements at TUM and at NTUA.	34
<b>Figure 29.</b> Relative power performance of the upstream turbine with respect to the no control case. NTUA: High Turbulence inflow, TUM: ABL inflow. Comparison between measurements at TUM and at NTUA.	35
<b>Figure 30.</b> Relative power performance of the upstream turbine with respect to the no control case. NTUA: High Turbulence inflow, TUM: ABL inflow. Comparison between measurements at TUM and at NTUA.	35
<b>Figure 31.</b> Relative power performance of the two turbines with respect to the no control case. Combination of Helix and Wake Steering (Static Yaw). Low turbulence inflow. Comparison between measurements at TUM and at NTUA.	36
<b>Figure 32.</b> Relative power performance of the upstream turbine with respect to the no control case. Combination of Helix and Wake Steering (Static Yaw). Low turbulence inflow. Comparison between measurements at TUM and at NTUA.	36
<b>Figure 33.</b> Relative power performance of the downstream turbine with respect to the no control case. Combination of Helix and Wake Steering (Static Yaw). Low turbulence inflow. Comparison between measurements at TUM and at NTUA.	37
<b>Figure 34.</b> Relative power performance of the two turbines with respect to the no control case. Combination of Helix and Wake Steering (Static Yaw). High turbulence inflow. Comparison between measurements at TUM and at NTUA.	38
<b>Figure 35.</b> Relative power performance of the upstream turbine with respect to the no control case. Combination of Helix and Wake Steering (Static Yaw). High turbulence inflow. Comparison between measurements at TUM and at NTUA.	38
<b>Figure 36.</b> Relative power performance of the downstream turbine with respect to the no control case. Combination of Helix and Wake Steering (Static Yaw). High turbulence inflow. Comparison between measurements at TUM and at NTUA.	38

# 1 Introduction

In the context of the TWEET-IE project, a twin-test is performed. One wind tunnel testing campaign is performed in the wind tunnel at the Technical University of Munich (TUM), Germany and a second test is performed at the National Technical University of Athens (NTUA), Greece. State-of-the-art measurement equipment from the Delft Technical University is used for the tests at NTUA. The tests concern the interaction between two wind turbine models and are focused on two specific wake control methods, namely helix and wake steering by static yaw misalignment. The objective is

- a. knowledge transfer between the partners and
- b. the creation of new knowledge on the topic of wake control and turbine interaction.

This chapter includes the description of the two facilities and equipment and outlines the relevant calibration procedures. In terms of results, a part of the acquired data is presented, focusing on the comparison between similar set ups at the two different wind tunnels and on the combination of the two wake control techniques.

## 2 TUM - Equipment and Methods. Training and Documentation

### 2.1 TUM Facility and equipment

#### 2.1.1 The wind tunnel at TUM

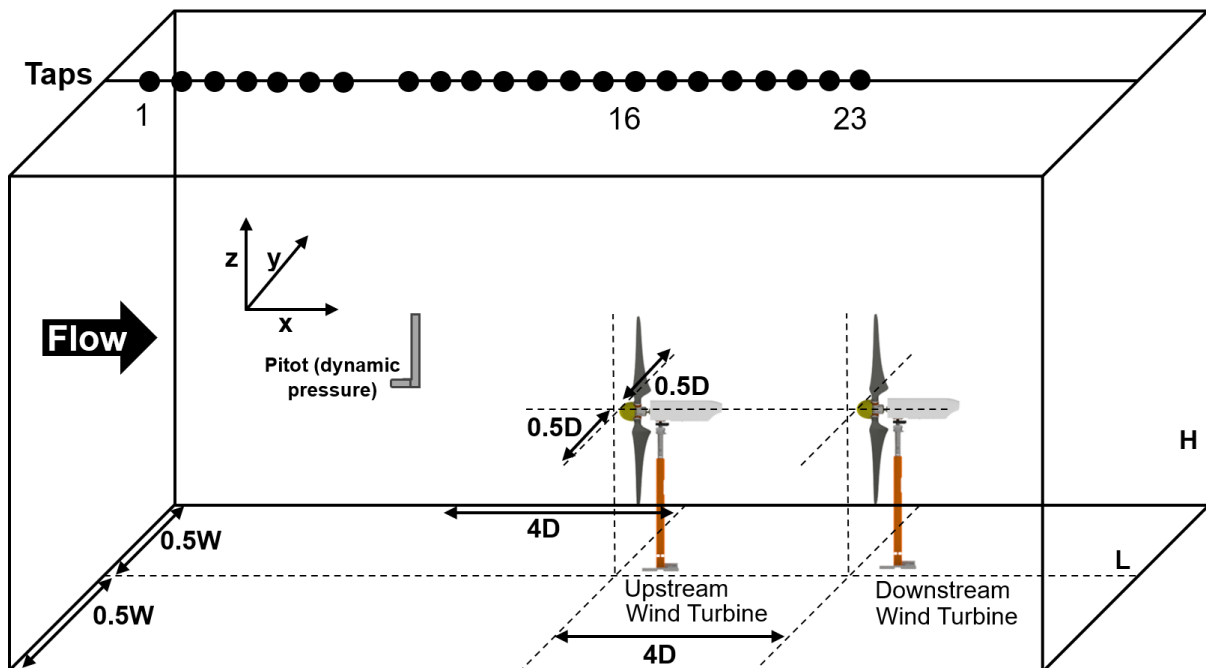
Measurements were conducted in the closed-loop, low-speed boundary layer wind tunnel of the Chair of Aerodynamics and Fluid Mechanics at Technische Universität München (TUM). This wind tunnel has a test section of: 21m (L) x 2.7m (W) x 1.8m (H), as presented in Figure 1. The blower is driven by a 210 kW electric motor, which allows velocity regulation from 1 m/s to 30 m/s. More technical details about the wind tunnel can be found in [1].

Figure 1 presents the static pressure taps located at the centre of the wind tunnel ceiling. This is an adjustable ceiling that enables an approximately zero pressure gradient to be obtained along the wind tunnel test section. The pressure taps coordinates in the streamwise (x, cm) and vertical (z, cm) directions are shown in Figure 2.  $\Delta P_{static, (i)}$  is defined as the difference between static pressure tap<sub>i</sub> and atmospheric pressure,

$$\Delta P_{static, i} = P_i - P_{atm} \quad (1)$$

The pressure measurements were recorded without and with wind turbine models within the test section for a time period of  $t_{empty} = 5 \text{ sec}$  and  $t_{models} = 5 \text{ sec}$ , respectively.

The tunnel wind speed is measured with a Pitot tube in a distance of  $4D$  upwind of the upstream wind turbine model (Figure 1). The pitot tube is located at hub height, 50cm from the tunnel side wall.



**Figure 1.** Sketch of the wind tunnel test section with the positioning of the pressure taps in the centre of the wind tunnel ceiling, the location of the pitot tube and the locations of the upstream and downstream wind turbine models.

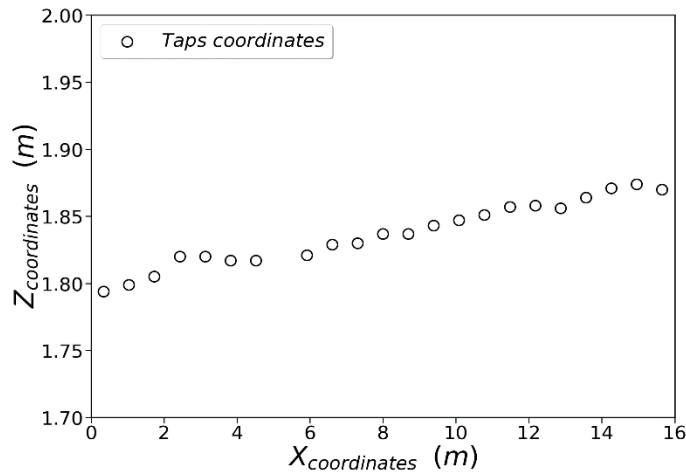


**Figure 2.** Streamwise (x, m) and vertical (z, m) coordinates of the pressure taps at different positions, along the centre of the wind tunnel ceiling; b).

### 2.1.2 Equipment

In addition to the sensors on the two wind turbine models a fast response aerodynamic probe (FRAP) was used to measure the velocity profiles at the locations of the two turbines and at the wake of the upstream one, when operating on its own. The probe was mounted on a traverse system to move between positions inside the test section.

The head of the FRAP probe is 3D printed, while its tip with a diameter of 3 mm is finished mechanically to guarantee small intrusivity. Pressure is measured by five differential piezo-resistive pressure sensors at the back of the probe head. Details about the probe and its application can be found in [2–4]. The FRAP is calibrated for its spatial and its temporal characteristics. The calibration allows for maximum flow angles of up to  $\pm 60^\circ$  and sampling frequencies of up to 10 kHz. Within this operational range, FRAP can achieve high accuracies of  $0.2^\circ$  for both flow angles and 0.1 m/s for the reconstructed velocity.



**Figure 3.** Fast-response five-hole probe equipped with piezo-resistive sensors, adapted from [2].

### 2.1.3 Inflow velocity and turbulence intensity profiles

The inflow velocity profile was measured directly at two locations inside the empty test section: firstly, the velocity profile was recorded at the position of the upstream wind turbine and secondly at the corresponding position of the downstream wind turbine model, as presented in Figure 1. Both instantaneous

velocity signals were measured at 14 points along a vertical line above the wind tunnel floor, without the turbine models in the test section. The velocity signal was sampled at 10 kHz for a total sampling time of 30s. Two main flow characteristics were determined: the mean wind velocity profile  $u(z)$  and the turbulence velocity profile  $TI_u(\%)$ , in the streamwise direction.

#### 2.1.4 Wind Turbine Models

The wind turbine models used in the blind test, are the G1 turbines, developed by TUM. A detailed description of the turbine design and applications are presented [5–7] while a detailed picture of the G1 turbine can be seen in **Figure 4**. The G1 features a rotor diameter,  $D = 1.1\text{ m}$ , a hub height of  $z_{hub} = 0.82\text{ m}$  and has a rated rotor speed,  $\omega = 850\text{ rpm}$  (clockwise rotation). Chord and twist distributions are given in Figure 5.

The turbines are heavily equipped with sensors and multiple actuators including individual pitch, torque and yaw control. The turbine performance can be acquired by various sensors that measure the shaft loads, shaft torque, tower loads, blade pitch, turbine yaw and rotor azimuth. The turbine is controlled by a Bachmann PLC, similar to that of full-scale machines. The full set of airfoil profiles, chord and pitch distributions and profile polars is available online with the measurement data.



**Figure 4.** The G1 wind turbine with highlighted components

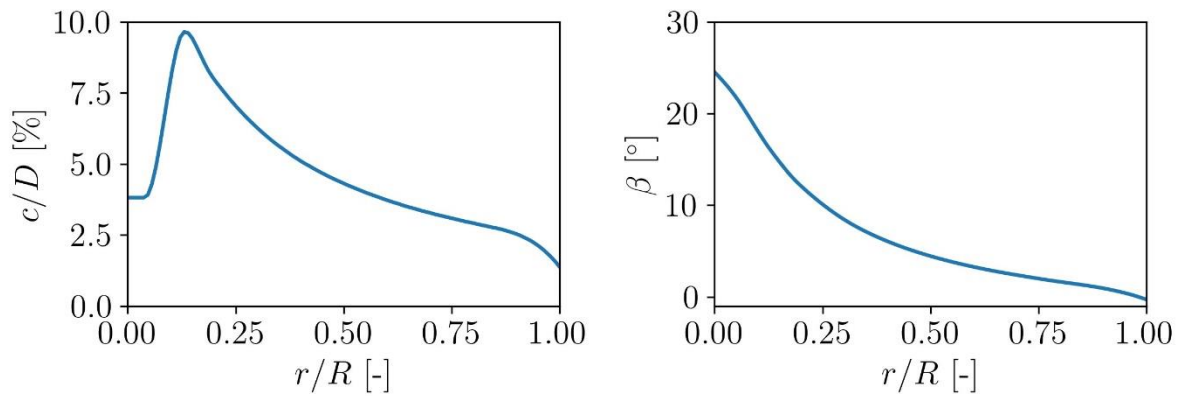


**Figure 5.** Chord and twist distribution for the G1 wind turbine model

### 2.1.5 Wind Turbine model calibration procedure

This section provides an overview of the calibration procedure for the G1 wind turbine models. Although the procedure is specific to the models used in this twin test the general methodology can be useful as a guide for other calibration procedures.

**Figure 6** and **Figure 7** show the orientation of the turbine parts and the needed tools for the calibration.

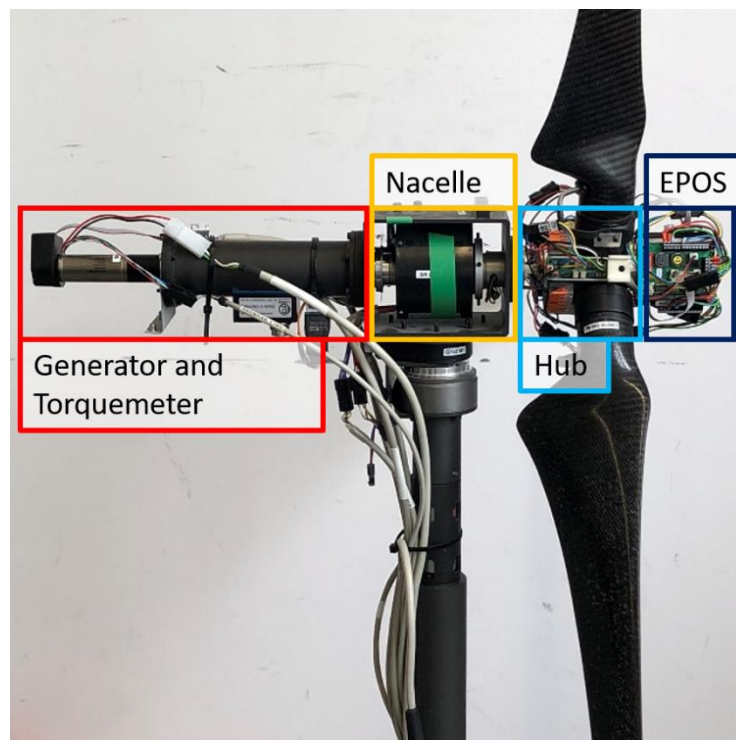


**Figure 6.** Orientation of the turbine parts



**Figure 7.** Tools needed for calibration

### 2.1.5.1 Task 1. Set-up

- Remove cover from hub
- Disconnect EPOS:
  - ▶ disconnect the cables coming from the blades and hub
  - ▶ unscrew EPOS with Allen key # 2.5
- Disconnect Rotor:
  - ▶ Disconnect the cables to the nacelle and remember the order
  - ▶ Unscrew Rotor with short Allen key # 3
- Fix rotor on the table with screw terminal and flatness tool
- Write down numbers of each Blade, blade root and hub connector configuration
- Remove blades from shaft:
  - ▶ Use special tool to unscrew each blade
- Fix hub onto table with screw terminal

### 2.1.5.2 Task 2: Blade calibration

Mount corresponding blade onto position 1 of the hub by using a hammer. (Caution: It's important to position pin correctly – Skrew-hole facing upwards)

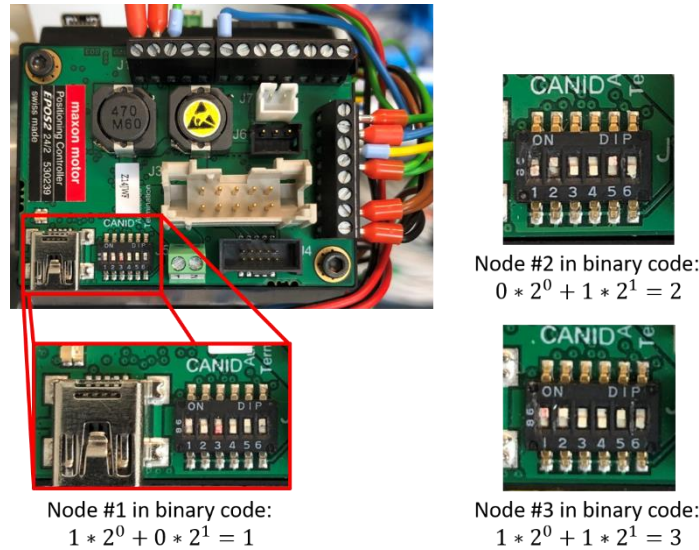


**Figure 8.** Binary numbering of nodes on EPOS

Find node #1 on the EPOS (Figure 8) and connect the USB cable from PC with port next to node numbering, the power cable from the Computer connection hub with the EPOS and all cables from the blade with the corresponding ports on the EPOS. (Caution with the power cable to connect red and black-black).

Set-up the inclinometer by placing it on a flat surface by standing parallel to the blades airfoils. Turn it on and press ‘Mode’ until the underscore is at ‘Zero’. Press ‘Enter’ and wait for the degree value to show up again. Press ‘Enter’ again to finalize the set-up.

Use the tape to fix the Inclinometer onto the blade-form tool.

In the following steps you will set up the computer for the calibration:

- Start EPOS Studio on PC:
  - ▶ Select EPOS2 Project and click “Next”
  - ▶ Click “Finish” -> check on top left side of the screen if you are connected to the correct mode
- Go to “Tools” -> “Device Control”
  - ▶ See that EPOS 2 ‘is disabled’
  - ▶ Click “disabled” -> Device ‘is enabled’
  - ▶ If Error: “Failed enabling device” comes up
    - Go to “Device Control”: Device ‘is in false state’
    - Click “Fault reset” -> Click “disable” -> Device ‘is enabled’
- Go to “Data recording” -> Click “Configure Recorder”
  - ▶ Channel 1: select Analog Input 1 -> left scale
  - ▶ Channel 2: select Analog Input 2 -> right scale
- Go to “Profile Position Mode”
  - ▶ Set Target Position to 100 and Click “Move Relative”
    - Mount blade-form-tool with inclinometer onto blade
    - Move blade to  $40^\circ \pm 1^\circ$
- Go to “Homing Mode” and click “Activate Homing Mode”

- ▶ Click “Start Homing” -> now 40° is set as our absolute zero position
- ▶ Click “Define Position”
- Go to “Profile Position Mode”
  - ▶ Click “Activate Profile Position Mode”
  - ▶ Click “ Move Absolute” after
    - Setting target position to 100 seeing on the inclinometer that the angle decreases
    - Setting target position back to 0 and seeing the inclinometer return to 40°
- Check data recording in EPOS Studio and log the Hall Output value into the table by looking at the ‘constant’ value of the Analog input 1 scale (read off  $\pm 1$ )
- Check angle of inclinometer and log it

Edit target position to the next value in the table (Caution: only move in steps of 100 as movement of blade is very fast) -> click “Move Absolute”

Repeat the previous two steps for all absolute positions in the table and save your table when you are done.

Perform calibration (Matlab or Excel)

Redo all the steps for the other two blades.

Remove the inclinometer from the blade. Disconnect the EPOS from the computer and the blade. Afterwards you remove the calibrated blade from the hub.

### 2.1.5.3 Task 3: Shaft calibration

For the shaft calibration you need to mount the turbine to the floor by using 3 bolts.

Detach the generator and torquemeter by unscrewing as shown in Figure 9 while fixing them afterwards to the tower by using a cable tie or Velcro fastener.

Remove the spring component by loosening its screw and mount the quadratic flat plate loosely onto the former position of the spring component.

Mount the hub onto nacelle and connect the cables from the nacelle.

Mount weight plate onto hub so that the horizontal position of the weight plate matches the position of the white tab (HUB #0X) showing towards the ceiling (BB2 facing upwards). Like this, blade 1 is facing upwards and the turbine is at Azimuth 0° (can be checked in Solution centre).

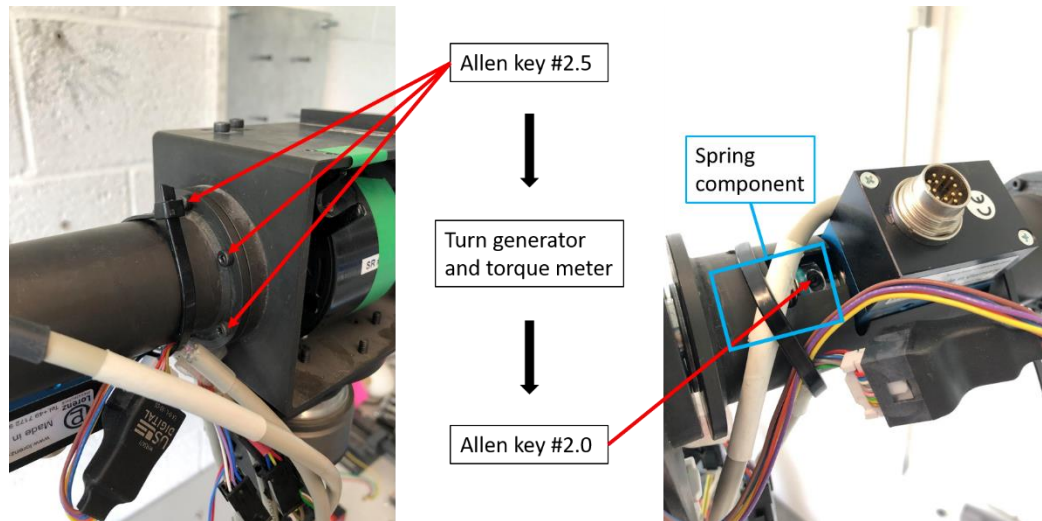


**Figure 9.** Detaching of the generator and torque meter

Set up the inclinometer again by placing it on a flat surface parallel to the weight plate surface and following the same steps as for the blade calibration.

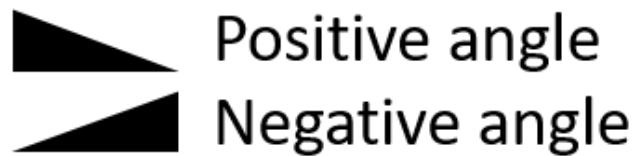


**Figure 10.** Sign of angles on inclinometer

Tighten the quadratic flat plate and position the weight plate at a small positive angle (see Figure 10) by taping the inclinometer onto the weight plate.

Check whether the quadratic flat plate is too tight or too loose:

- Hang heaviest weight onto the 60 position of the weight plate (see Figure 11)
  - ▶ Quadratic flat plate is tight enough if initial angle at inclinometer and angle after removing the weight are the same
  - ▶ Quadratic flat plate is too tight if initial angle at inclinometer does not change

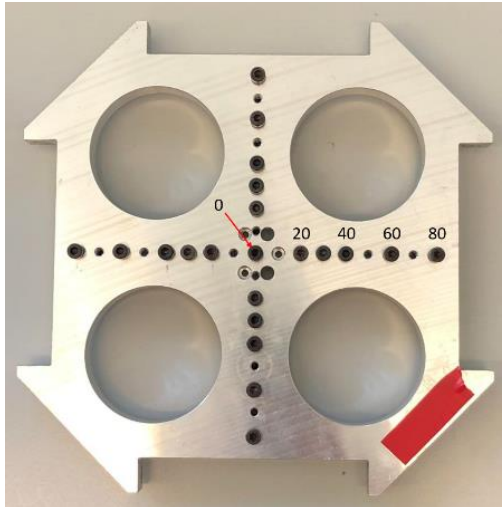


Figure 11. Positions on the weight plate

Turn on the Bachman (ask Tutor) and connect the EPOS to the hub via the cables. The green light on the EPOS should light up.

Use the software (Bachmann) for shaft calibration.

- Open Solution Center and select 'D:\Bachmann\Local'. Click "Launch" and go to GXv2 (or My Devices) -> This is the connection between the Bachman and the computer
  - ▶ Check if model is online (Green dot next to m205 (TCP))
- Go to bottom (or right) screen and open the FTP tab:
  - ▶ Go to REMOTE:
    - Select folder of your model
    - Go to usbBulk0 / Data
    - Check if files: Calibration\_Average.dat & Calibration\_Raw\_Data.bin are present in the Data folder
    - If they are: delete them. If not: continue

As the computer is set up you can start calibrating the shaft:

- Open Firefox and go to URL 10.152.168.(Bachmann\_number):8080
  - ▶ Click "Calibr" and select "Shaft"
  - ▶ Click "Activate"
  - ▶ Click "Remove off-set"
  - ▶ Define Parameters
 

▪ Azimuth Angle:	inclinometer value
▪ Theta:	inclinometer value
▪ Distance Axial:	88
▪ Distance Lateral:	80
▪ Vertical weight:	Read label on weight (Start with lightest)
- (2000 g, 1000 g and 500 g)
  - ▶ Recording:
    - Hang weight onto 80 position of weight plate and wait until it stops oscillating
    - Click "Start recording"
    - Change Distance Lateral to 60
    - Remove weight and check if inclinometer goes back to initial angle

- Hang weight onto 60 position of weight plate
- Click “Start recording”
- Redo Recording steps for lateral distances of 40, 20 and 0
- Increase the Vertical weight parameter and redo Recording steps with heavier weights (The 2 kg weight starts at Distance Lateral 60 instead of 80)
- Go to Solution Center and refresh REMOTE Data
  - ▶ 2 new files have been created: Calibration\_Average.dat & Calibration\_Raw\_Data.bin

At this stage of the calibration you would continue calibrating for the 90, 180 and 270 position of the weight plate. However, we provide you the measurement data for the other positions due to our limited time of this exercise.

Find the file “Calibration\_Average\_Data\_old.dat” in the shaft folder and follow the instructions in the file.

Open the Matlab script “G1v2\_Calibration\_Read\_Bachmann\_Data.m” and run it. Don’t be bothered by the other files as they are simply used by the Matlab script but are not relevant for your task.

Write down the Error values in percent for torque, nodding and side-side calibration.

Reduce error by excluding problematic measurements:

- Go to line 28 and set flag.Exclude\_Lines = 0; to = 1;
- Fill array ‘Exclude\_Lines’ with x-coordinates of highest peaks in error graphs (fig 11 on Torque, Nodding and SideSide Error)
- Rerun code and see that the error has been reduced

Detach the weight plate and the quadratic flat plate and mount the generator and torquemeter back onto the nacelle.

#### 2.1.5.4 Task 4: Tower calibration

Mount the EPOS onto the hub and connect them via their cables.

Mount the tower onto the wall and turn on the Bachman.

- CAUTION as EPOS will rotate for 3 seconds

Set up the inclinometer on a flat surface while facing away from the wall by following the same steps as for the blade calibration. Place the inclinometer as shown in Figure 12 and note down the measurement.



**Figure 12.** Position of inclinometer for tower calibration

Set up the computer for the tower calibration:

- Open Solution Center and go to GXv2 (or My Devices)
  - ▶ Check if model is online (Green dot next to m205 (TCP))
- Go to bottom (or right) screen and open the FTP tab:
  - ▶ Go to REMOTE:
    - Select folder of your model
    - Go to usbBulk0 / Data
    - Check if files: Calibration\_Average.dat & Calibration\_Raw\_Data.bin are present in the Data folder
    - If they are: delete them. If not: continue

Set up you can start calibrating the tower:

- Open Firefox and go to URL 10.152.168.(Bachmann\_number):8080
  - ▶ Click “Calibr” and select “Tower”
  - ▶ Click “Activate”
  - ▶ Click “Remove Offset” (without the hook on the tower)
  - ▶ Define parameters:
    - Gamma                      Value of inclinometer
    - Theta:                      Value of inclinometer
  - ▶ Attach hook onto tower at the upper end of the bottom tube (magnetic)
  - ▶ Measure the distance from middle of strain gauges at the root of the tower to position of the hook (~ 460 mm)
  - ▶ Define Axial Distance:      Measurement from previous step
  - ▶ Remove Hook
  - ▶ Click “Start Recording” -> Zero weight configuration
  - ▶ Define Hook weight:        Written on hook
  - ▶ Define Vertical weight:      Label on weight
  - ▶ Attach hook onto same position as before

- ▶ Hang weight onto hook and wait until the weight stops oscillating
- ▶ Click “Start Recording”
- ▶ Remove weight and attach heavier weight onto hook
- ▶ Redefine the Vertical weight:           Label on weight
- ▶ Click “Start recording”
- ▶ Redo the last 3 steps for all weights (2000 g, 1000 g and 500 g)

For completing the tower calibration it would be necessary to calibrate the tower in its 90, 180 and 270 position as well. The steps are exactly the same only the position on the wall changes. As before we provide you the measurement data for the other positions.

Find the file “Calibration\_Average\_Data\_old\_tower.dat” in the tower folder and follow the instructions in the file.

Open and run the Matlab script “G1v2\_Calibration\_Read\_Bachmann\_Data.m”.

Look at the Error values in percent for nodding and side-side calibration and check if they are under 0.5.

### 3 NTUA - Equipment and methods. Applied knowledge.

#### 3.1 The NTUA wind tunnel set up

The wind tunnel experiments were carried-out in the large section  $2.5 \times 3.5 \times 12\text{m}^3$  ( $H \times W \times L$ ) of the closed-circuit wind tunnel at NTUA, see also Section TWT1, Section 4.1.2. The set up consists of two identically scaled wind turbine models (G1 models) which are placed in line with a longitudinal distance of  $5D$ , see Figure 13.

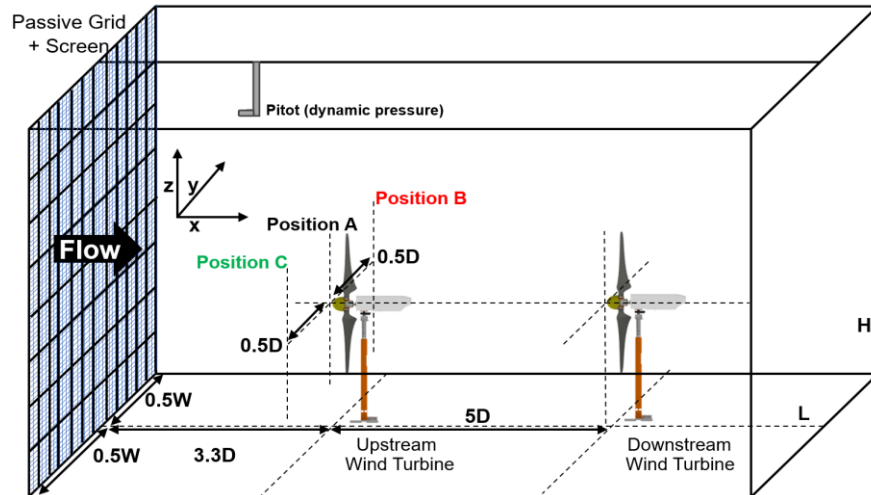


**Figure 13.** Sketch of the NTUA wind tunnel test section with the location of the pitot tube and the locations of the upstream and downstream wind turbine models, when high turbulence intensity (screen and passive grid) is applied (not to scale).

#### 3.2 Inflow

Both low turbulence ( $T.I. \approx 1.5\%$ ) and high turbulence ( $T.I. \approx 6\%$ ) inflow conditions were tested. The latter was achieved by adding a passive turbulence grid at the test section inlet, see **Figure 14**. The wooden bars had a cross section of  $24\text{mm} \times 48\text{mm}$ . The distance between the centres of the bars was  $30\text{cm}$ .



**Figure 14.** Upstream view of the test section with the passive grid installed.

### 3.3 Hot Wire Anemometry

The inflow profile was measured using a TSI Inc. IFA 300 measurement system with a single wire probe (TSI 1201, see Figure 15), that was calibrated in-situ prior to the measurements. The sampling frequency was 10 kHz with a low pass filter at 5k Hz and a sampling time of 104 seconds. For the calibration function use a 4<sup>th</sup> order polynomial was used and a temperature correction according to the manufacturer was applied.

The inflow velocity was measured vertically at locations A, B and C, as shown in *Figure 13* and vertically at hub height. The uncertainty for the hot wire measurements was <2%.

### Model 1201 Disposable Probe

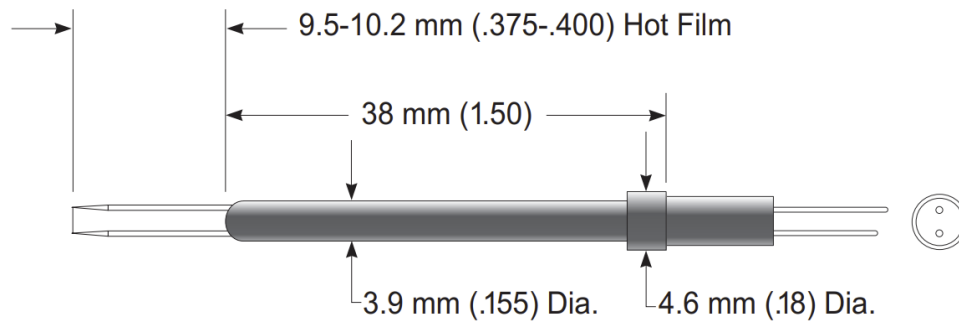


**Figure 15.** Single wire sensor used for the inflow measurements.

## 3.4 Particle Tracking Velocimetry

### 3.4.1 Equipment

#### 3.4.1.1 Cameras

Three high-speed Photron Fastcam SA1.1 cameras (see Figure 16) were used in the PTV setup with a sensor resolution of 1024X1024 and a pixel size of 20X20 $\mu$ m. The maximum acquisition frequency of the cameras is 5400 Hz at full resolution. The cameras were mounted on X95 beams in the configuration illustrated in Figure 17.



**Figure 16.** A Photron Fastcam SA1.1 camera

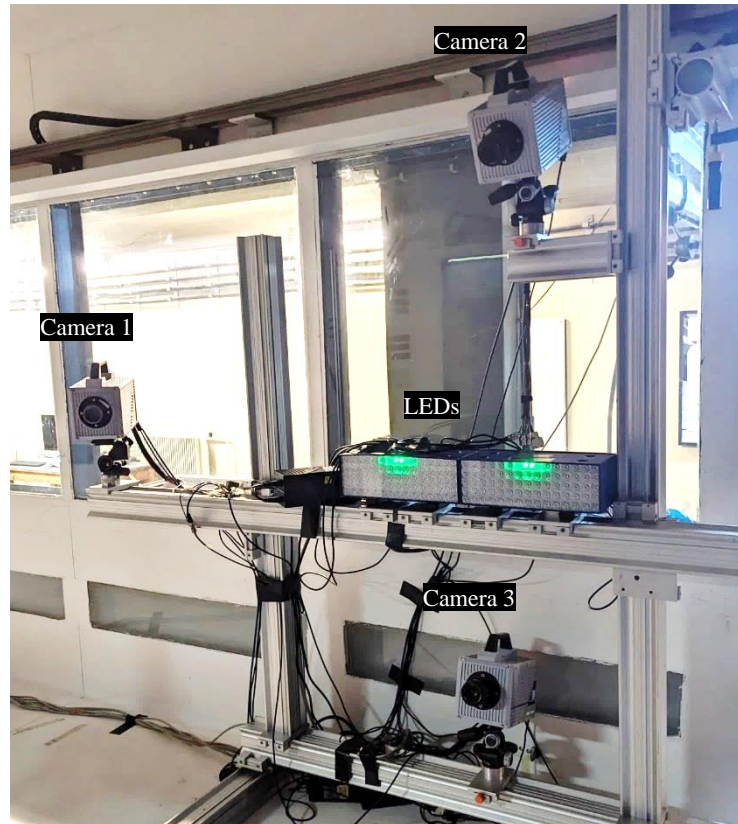


**Figure 17.** Camera Setup inside the test section

The cameras used Nikkor lenses, two with a focal length of 35 mm and one with a focal length of 50 mm. The numerical aperture of the lenses was set to  $f\# = 16$ . For the experiment, the PTV images were acquired at a frequency of 1000Hz. The number of images acquired in each acquisition and the number of repetitions per acquisition varied depending on the tested configuration (presence of helix and/or yaw). A high-speed ethernet cable was used to transfer data from the cameras to the acquisition computer. The imaged measurement domain was  $1100 \times 720 \times 400 \text{ mm}^3$ , resulting in a magnification factor  $M = 0.018$  and a digital image resolution of 1.41 px/mm.

### 3.4.1.2 High-speed Controller

The Programmable Timing Unit (PTU) X was used to synchronize the illumination from the LED and the acquisition from the cameras, see Figure 18. Additionally, the PTU-X received a trigger signal (sent via a coaxial cable) from the wind turbine at a specific azimuth and phase of the helix, so that all the measurements could start in the same condition.



**Figure 18.** A PTU-X, by LaVision

### 3.4.1.3 Illumination

Two LaVision LED Flashlight 300s (see **Figure 19**) were used to provide pulsed volumetric illumination. Each module consists of an array of 72 high-power LEDs in an area of  $300 \times 100 \text{ mm}^2$ . The incoherent white light ensures high image quality with constant homogeneous brightness in time and space. The LEDs have an operating angle of  $10^\circ$  and a maximum operating frequency of 20kHz. The LEDs can be operated in continuous mode or pulsed mode depending on the applications.



**Figure 19.** LED Flashlight 300

To minimize the amount of unwanted background light reflections, the wall of the wind tunnel opposite to the cameras was covered with dark (black and blue) paper sheets. Additionally, the paper sheets were painted with Musou Black paint, which has a nominal absorptivity of 99.4% of light in the visible range (source: <https://www.musoublack.com/> ).

### 3.4.1.4 Seeding rake and Fluid Supply Unit (FSU)

The seeding rake (see Figure 20) generates neutrally-buoyant Helium-filled soap bubbles of  $300 \mu\text{m}$  median diameter, used as tracer particles for PTV. The seeding rake consists of 200 bubble generators arranged on 10 parallel wings of 1m each. The seeding surface area is approximately  $0.5 \times 0.95 \text{ m}^2$ . The Fluid Supply Unity (FSU) controls the pressures of Helium, air, and soap solution, which can be fine-tuned to adjust the size and number of bubbles produced by the seeding rake. During the measurements, the pressures were kept at 2.5 bar for air and 2 bar for both He and soap.



Figure 20. Seeding rake in the wind tunnel test section

### 3.4.2 *PTV System Calibration*

The PTV system needs to be calibrated before measurements can be made. The calibration procedure consists of two steps: Geometric Calibration and Volumetric Self Calibration

#### 3.4.2.1 *Geometric Calibration*

Geometric calibration is performed to compute a mapping function from real-world space to camera sensor plane and correct for distortions and oblique views. For 3D PTV, geometric calibration is performed using a standard calibration plate (see Figure 21).

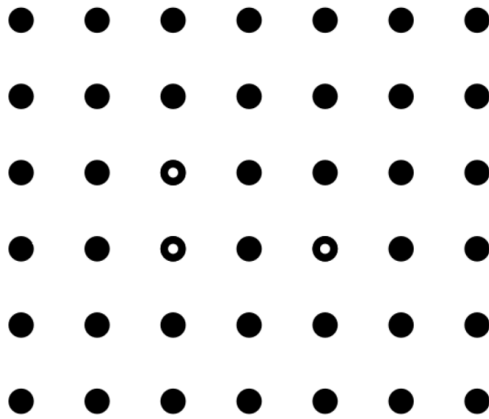


Figure 21. Calibration plate 395-54 SSSP used for the geometric calibration.

Once the appropriate calibration plate is selected in the DaVis calibration dialog, the number of marks, their size, and their distances are known. The calibration plate used for the experiment is the 395-54 SSSP. The plate has 42 markers spaced 54mm apart, a width of 395mm and a height of 342mm. There are three open circles, called fiducials, which define the orientation of the calibration plate and also define the coordinate system.

The geometric calibration procedure is as follows:

- Place the calibration plate at approximately the center of the measurement domain. This first position corresponds to  $z=0$  position of the measurement domain. Images of the calibration plate are captured from each camera.
- The calibration plate is moved in the depth direction ( $z$ -axis)  $\pm 150$ mm and images are captured from each camera for each position of the calibration plate.
- The images captured for the different calibration plate positions are then used by DaVis to automatically compute the mapping function from 3D space to the image space for each camera.

#### 3.4.2.2 Volume Self-calibration

Volume Self-calibration is a technique to detect and correct calibration disparities in 3D-PTV experiments. Starting from a plate-based calibration, volume self-calibration makes use of the recorded particle images to detect and correct calibration errors [8].

First, the measurement volume is subdivided into several sub-volumes. Within each sub-volume, the average disparity is computed and a disparity vector map is generated. Based on the disparity vector map, a correction to the calibration is applied. These steps are repeated until the disparity within each sub-volume is below 0.1 voxel.

The Optical Transfer Function (OTF) can be calculated once the Volume Self-Calibration is performed. An elliptical Gaussian model is fitted for each sub-volume and each camera to represent the OTF [9].

#### 3.4.3 PTV Data Analysis

The acquired images are first pre-processed via subtraction of the time-minimum intensity on a slide kernel of 5 images to remove any unwanted light reflections. Successively, Lagrangian Particle Tracking is performed using the Shake-the-Box algorithm [10].

### 3.5 Wake control techniques

For the NTUA tests, the upstream turbine was actuated following three control strategies:

- i. the *Helix* approach, where the wind turbine blades experience a dynamic individual pitch control/excitation (DIPC) resulting in a variation of the fixed-frame tilt and yaw moments and a dynamically variation of the direction of the thrust force.
- ii. the *Static yaw* as a wake steering control strategy in which upstream turbine operates with a yaw misalignment to deflect their wakes away from downstream turbine, yielding a net power gain (for the wind plant case), and
- iii. the combination of both control strategies: *Helix with Static Yaw*.

The downstream turbine acts purely as a sensor, providing an integral insight on the energy content in the wake and thus the recovery behind the first turbine.

During this experimental investigation, all Helix tests (individual or as a combination) were conducted by solely changing the additional pitch excitation frequency  $f_e$ , which is controlled by setting a desired pitch frequency,  $f_\beta$  in the wind turbine software interface controller. The blades are individually controlled with a sinusoidal excitation with a frequency  $f_\beta = f_r \pm f_e$ , which is out of sync with the rotational frequency  $f_r = \omega_r / 60 = 1P$ . The additional excitation frequency  $f_e$  is either added or subtracted to the rotational frequency, leading to the counterclockwise [CCW] or clockwise [CW] wake meandering, respectively.

During the tests,  $f_\beta$  was varied within the range of 9.92 – 18.47 Hz with a step of 0.57 Hz. The upstream wind turbine is operated at a constant rotational frequency of  $f_r = 850 \text{ rpm} / 60 = 14.1667 \text{ Hz}$  and an optimal pitch offset of  $\beta_o = 0.4^\circ$ . These controls result in a non-dimensional actuation frequency of  $f_\beta / f_r$  with values vary between 0.70 – 1.30, having a step of 0.04, which correspond to a Strouhal number defined in terms of additional frequency as  $St_{add} = \frac{f_e D}{U_{Pitot}}$ , where  $D$  is the rotor diameter. The Strouhal number  $St_{add}$ , is in the range of 0.053 – 0.792 with a step of 0.106.

## 4 Twin Test 2: Wake interactions of a cluster of turbines and wake steering techniques

### 4.1 TUM Results

#### 4.1.1 Pressure variation along the test section

Figure 22 shows the pressure drop along the free stream direction for a wind speed of 5.74 m/s for an empty test section and when the two turbine models are installed and operational. In the latter case, the upstream turbine model operating at  $\omega_{upstream} = 850 \text{ rpm}$  and the downstream turbine operating at  $\omega_{downstream} = 574 \text{ rpm}$ .

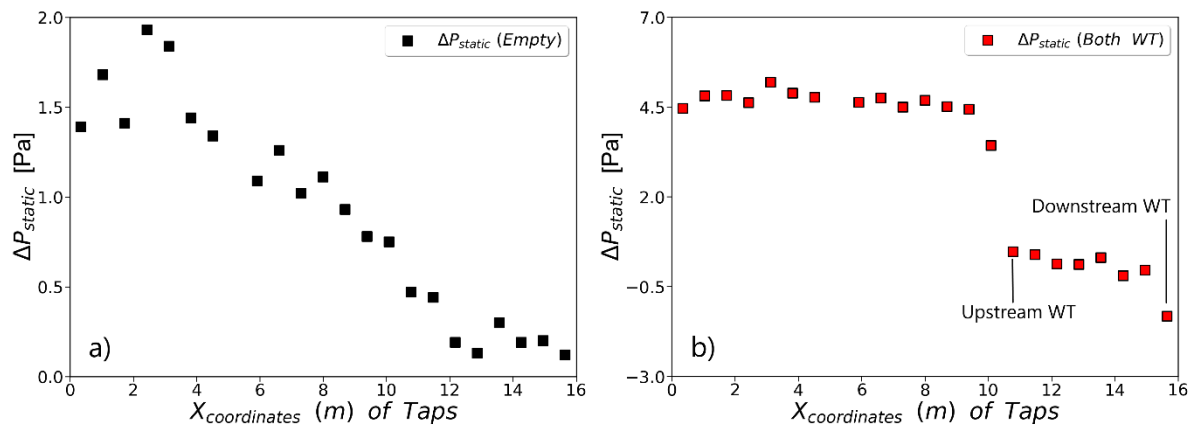


**Figure 22.** Pressure drop along the ceiling of the test section (in the streamwise direction): a) without wind turbine models in the wind tunnel test section and b) with both wind turbine models installed: the upstream turbine model operates at  $\omega_{upstream} = 850 \text{ rpm}$  while the downstream turbine model operates at  $\omega_{downstream} = 574 \text{ rpm}$ .

In the case of the empty wind tunnel (Figure 22a) the pressure drop is less than 2 Pa in 16 m which is considered good. In the case of the operating wind turbines (Figure 22b) the presence of the two models is clearly registered in the recorded pressures, with an increase of the pressure from the inlet and a sudden drop upstream of each wind turbine model, as expected [11]

## 4.1.2 Inflow velocity and turbulence intensity profiles

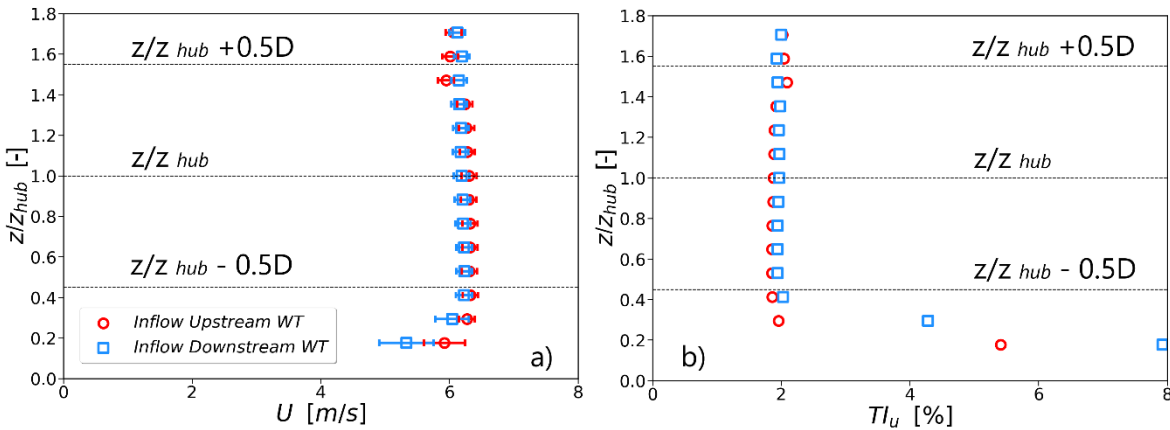
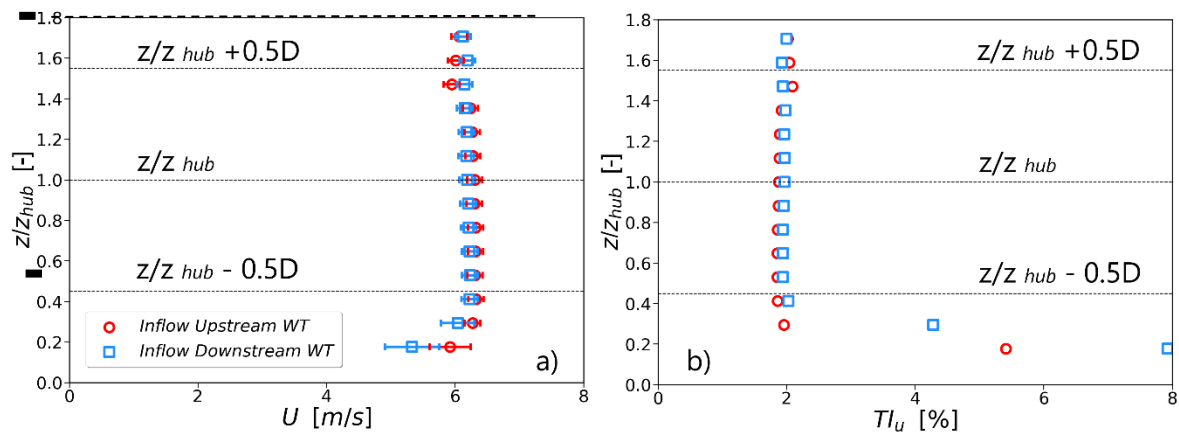


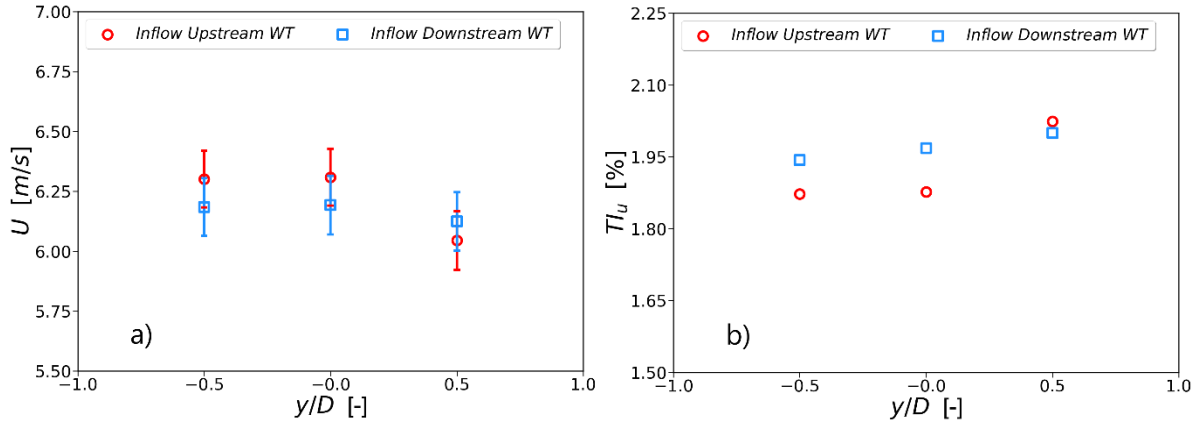
Figure 23 presents the velocity and turbulence intensity profiles in the empty wind tunnel test section at two locations: at the position of the upstream wind turbine and at the downstream wind turbine model. The measurements show a uniform streamwise velocity profile at both locations for  $z/z_{hub} \geq 0.35$ . The boundary layer on the tunnel floor grows with distance as expected.

Figure 5b presents the streamwise turbulence intensity profile  $TI_u$  (%) calculated at the positions of the upstream and downstream turbine models. The turbulence intensity at hub height is 1.88% for the upstream turbine model and 1.97% for the downstream turbine model. Within the boundary layer height,  $\delta$  i.e.  $z < 30$  cm,  $TI_u$  values are higher (between 4% and 8%), again as expected.



**Figure 23.** Vertical inflow profiles of a) streamwise velocity  $U$  (m/s) (error bars: standard deviation of streamwise velocity); and b) turbulence intensity,  $TI_u$  (%) in the empty wind tunnel test section, at the positions of the two wind turbine models.

Additional velocity measurements were performed at hub height, at two additional points in the lateral direction ( $y = \pm 0.5D$ ) to examine the symmetry of the inflow streamwise velocity and the turbulence intensity at the locations of the two models, see Figure 24. A marginal asymmetry of the inflow profile and turbulence intensity at the location of the upstream profile appears to be diffused at the downstream turbine location.



**Figure 24.** a) Streamwise velocity,  $u$  (m/s) and b) Turbulence intensity,  $TI_u$  (%) variation along the spanwise direction in the empty wind tunnel test section, at the positions of the two wind turbine models.

### 4.1.3 Wind Turbine Performance

The performance of the two turbines was examined independently, with each model located on its own in the wind tunnel, and in tandem with each other, i.e. with both models operating in the test section. When the models are operating on their own, they are at the same location as when they are both installed in the wind tunnel, see Figure 1. It is noted that in all cases the velocity calculated by the pitot tube measurements is used for the calculation of both coefficients and tip speed ratios.

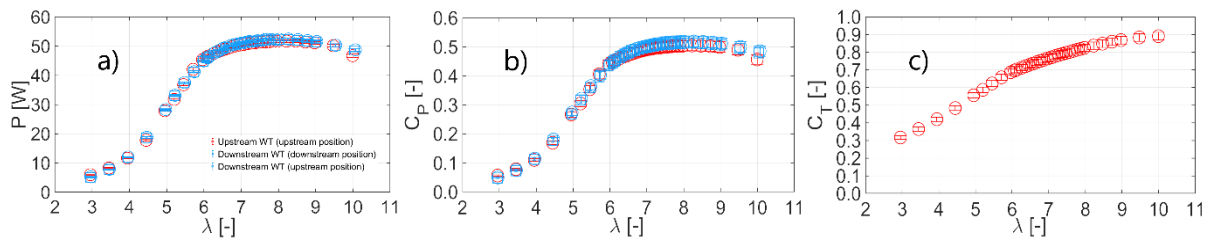


**Figure 25.** a) Power,  $P$ ; b) power coefficient,  $C_p$ ; and c) thrust coefficient  $C_T$  variation with tip speed ratio,  $\lambda$ , when each of the turbine models is placed independently in the wind tunnel test section.

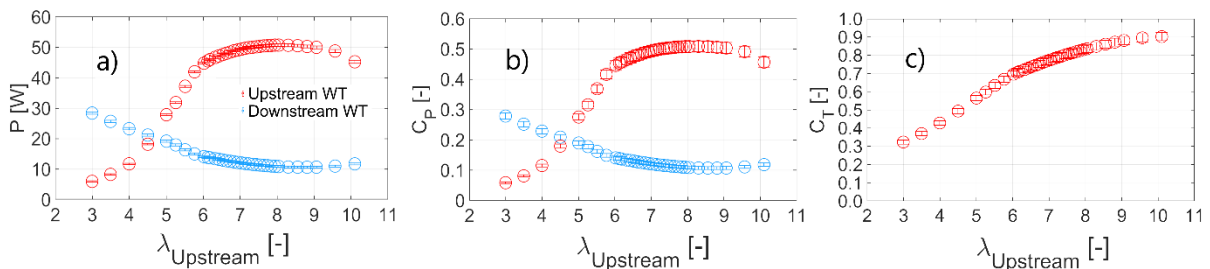


**Figure 26.** a) Power,  $P$ ; b) power coefficient,  $C_p$ ; and c) thrust coefficient  $C_T$  variation with upstream turbine tip speed ratio,  $\lambda_{upstream}$ , when both wind turbines are placed in the wind tunnel test section. The upstream wind turbine model rotates at variable rotational speed while the downstream wind turbine rotates at constant rotor speed (574 rpm,  $\lambda_{downstream} = 5.86$ ).

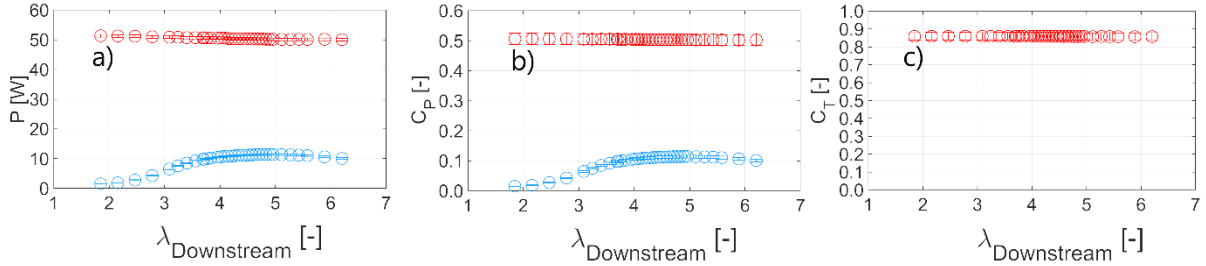


**Figure 27.** a) Power,  $P$ ; b) power coefficient,  $C_p$ ; and c) thrust coefficient  $C_T$  variation with downstream turbine tip speed ratio,  $\lambda_{downstream}$ , when both wind turbines are placed in the wind tunnel test section. The upstream wind turbine model rotates at constant rotational speed (850 rpm,  $\lambda_{upstream} = 8.53$ ) while the downstream wind turbine rotates at variable rotor speed.

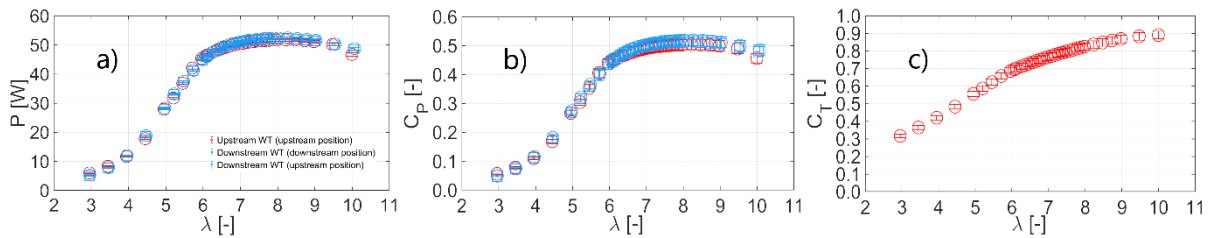


Figure 25 shows the power, power coefficient and thrust coefficient variation with tip speed ratio when each model is operating on its own. The turbine performances are very similar and any discrepancies are attributed to the different ways of calculating Power. For the upstream turbine, the shaft strain gauge measurements are used, while for the downstream turbine the friction corrected torque sensor measurements are used. Thrust was derived based on strain gauge measurement at the tower base.

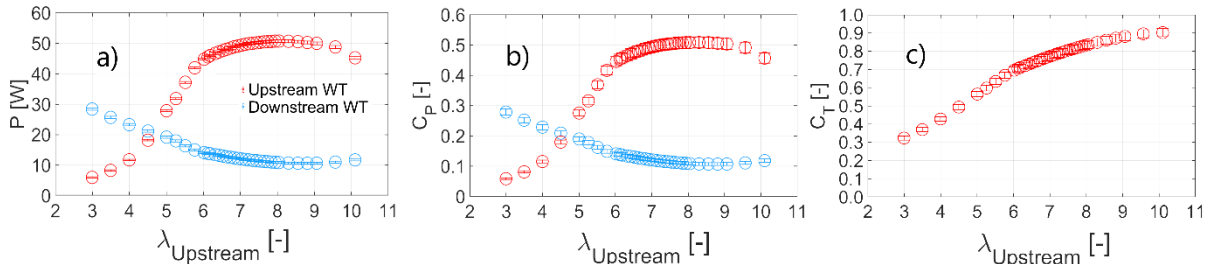


Figure 26 shows the performance of both turbines against  $\lambda_{upstream}$ , when the upstream and downstream turbines operate at variable and constant RPM, respectively. Clearly, the performance of the upstream turbine and the energy extracted from the flow significantly affect the performance of the downstream one.

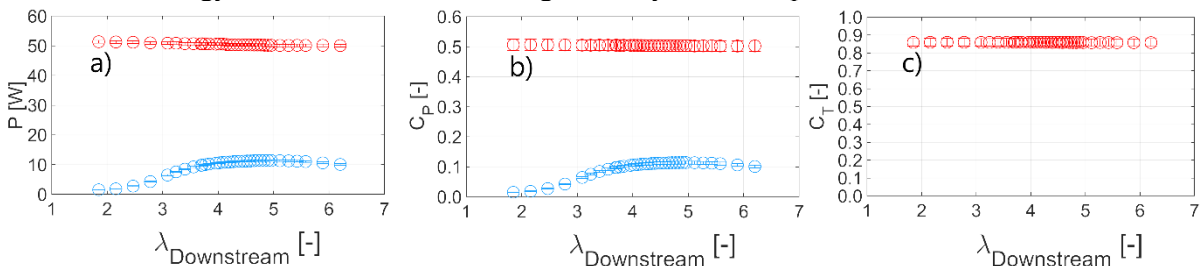


Figure 27 presents the performance of the two turbines when the upstream one operates at constant RPM and the downstream one operates at variable RPM. The upstream turbine remains largely unaffected while the downstream turbine displays peak performance at  $\lambda_{downstream} = 5.1$ .

The baseline case is considered that where the upstream and downstream turbine operate at 849 RPM and 637 RPM, respectively, the tunnel wind speed is 5.72 m/s. For this case the expected performance is given in Table 1.

**Table 1.** Performance of the two wind turbines for the baseline case

	Rotational Speed	Power	Power Uncertainty	$C_p$	$C_p$ uncertainty	$C_T$	$C_T$ uncertainty
Turbine	RPM	[W]	[±W]	[-]	[±]	[-]	[±]
<i>Upstream</i>	850	44.6	0.45	0.50	0.02	0.88	0.02
<i>Downstream</i>	544	9.5	0.28	0.11	0.005	0.33	0.01

## 4.2 NTUA Results

In this section, the results from the NTUA measurements are presented and compared to the relevant measurements from the TUM tests, where applicable. Please note that for the low turbulence inflow case T.I.=2% at TUM and T.I.=1.5% at NTUA. Also, for the high turbulence, an Atmospheric Boundary Layer profile was used at TUM with max T.I.≈6%, while a uniform profile with T.I.=6% was employed at NTUA.

### 4.2.1 Inflow

The vertical velocity profiles at three different locations for the low and high turbulence intensity conditions are shown in Figure 28 and Figure 29, respectively. The relevant horizontal profile at hub height is given in Figure 30. The flow homogeneity is considered good and the level of difference between the low and high T.I. levels large enough to provide meaningful comparisons.

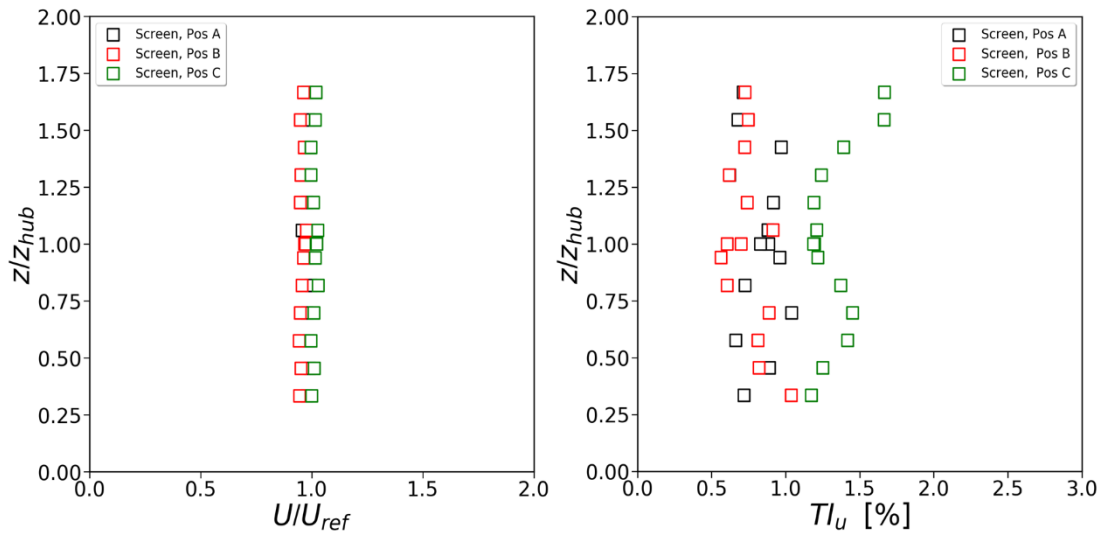


**Figure 28.** Low turbulence case. Inflow velocity and turbulence intensity profiles at the location of the wind turbine rotor at locations A, B and C as indicated in Figure 13.

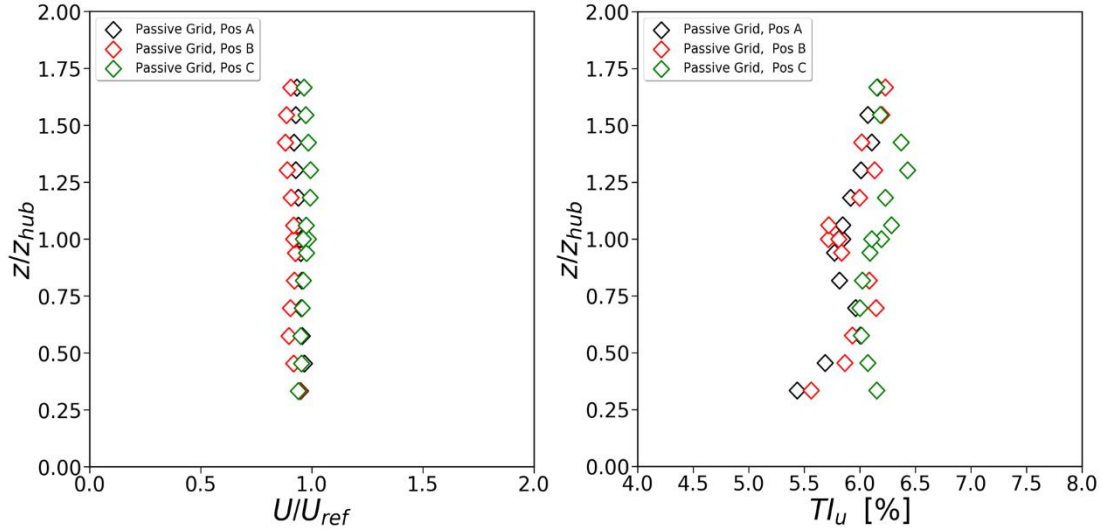


**Figure 29.** High turbulence case. Inflow velocity and turbulence intensity profiles at the location of the wind turbine rotor at locations A, B and C as indicated in *Figure 13*.

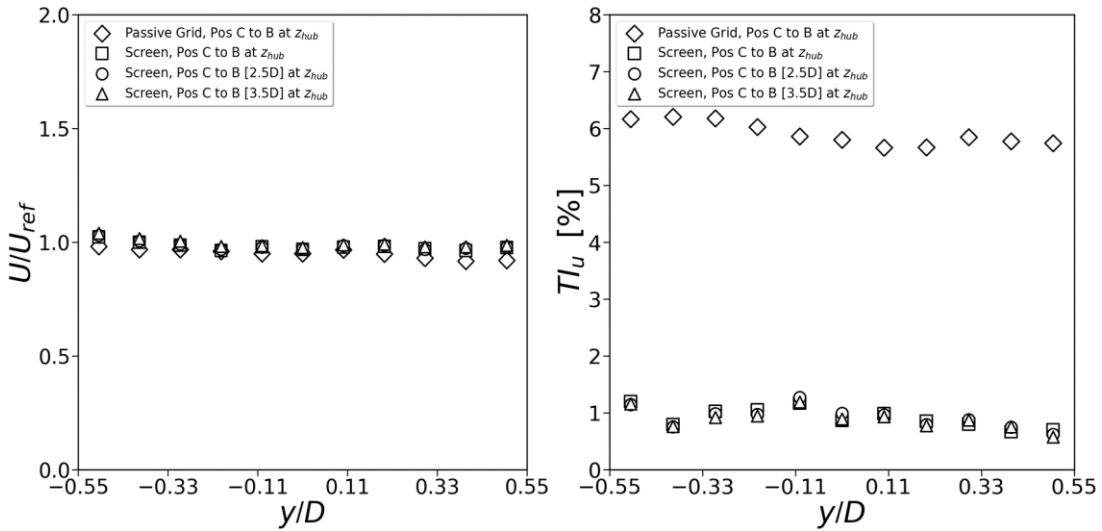


**Figure 30.** Horizontal inflow velocity and turbulence intensity profiles at hub height between positions B and C, as indicated in *Figure 13*.

#### 4.2.2 Helix, Low Turbulence – Comparison with TUM results

Figure 31 shows the relative performance of the two turbines when the helix control is applied with respect to the no control case. Figure 32 and Figure 33 present the same quantity for the upstream and downstream turbine respectively. The comparison for the wind farm case (both wind turbines) is very good and the variation of power with  $f_{helix}$  shows the same trends.

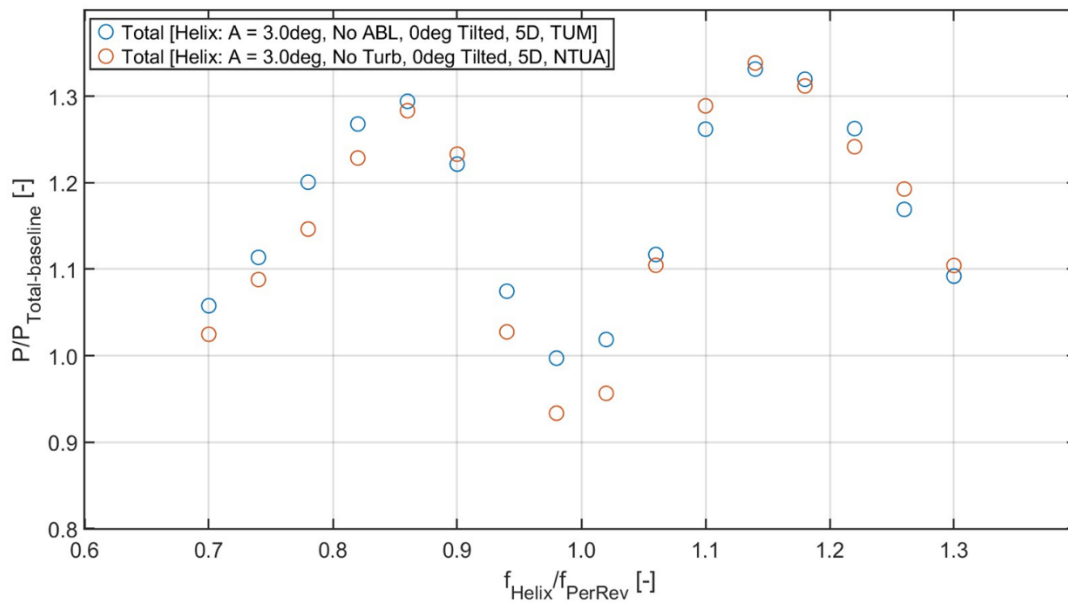


**Figure 31.** Relative power performance of the two turbines with respect to the no control case. Comparison between measurements at TUM and at NTUA.

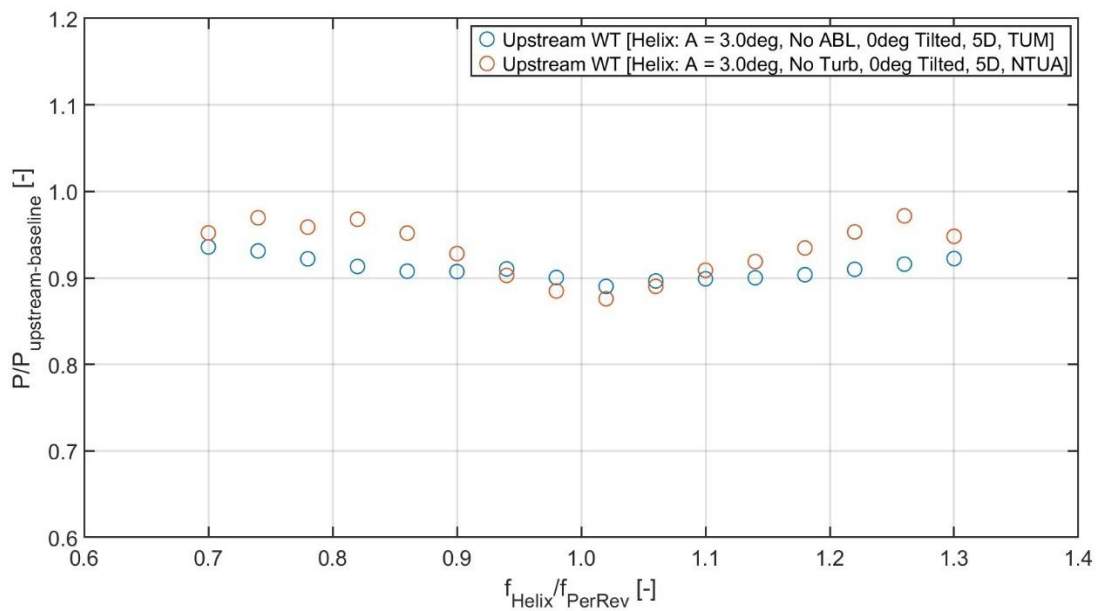


**Figure 32.** Relative power performance of the upstream turbine with respect to the no control case. Comparison between measurements at TUM and at NTUA.

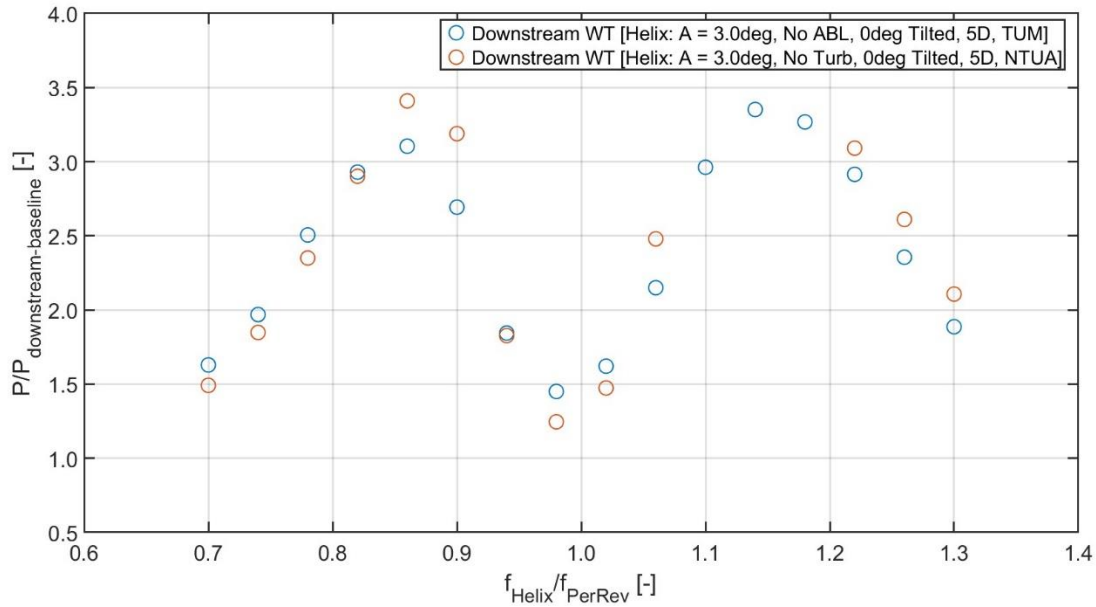


**Figure 33.** Relative power performance of the downstream turbine with respect to the no control case. Comparison between measurements at TUM and at NTUA.

#### 4.2.3 Helix, High Turbulence – Comparison with TUM results

High turbulence inflow results also compare very well between the two facilities as show in Figure 34, Figure 35 and Figure 36. Helix wake control effect and trends are similar and compare very well with very recent literature [4,12].

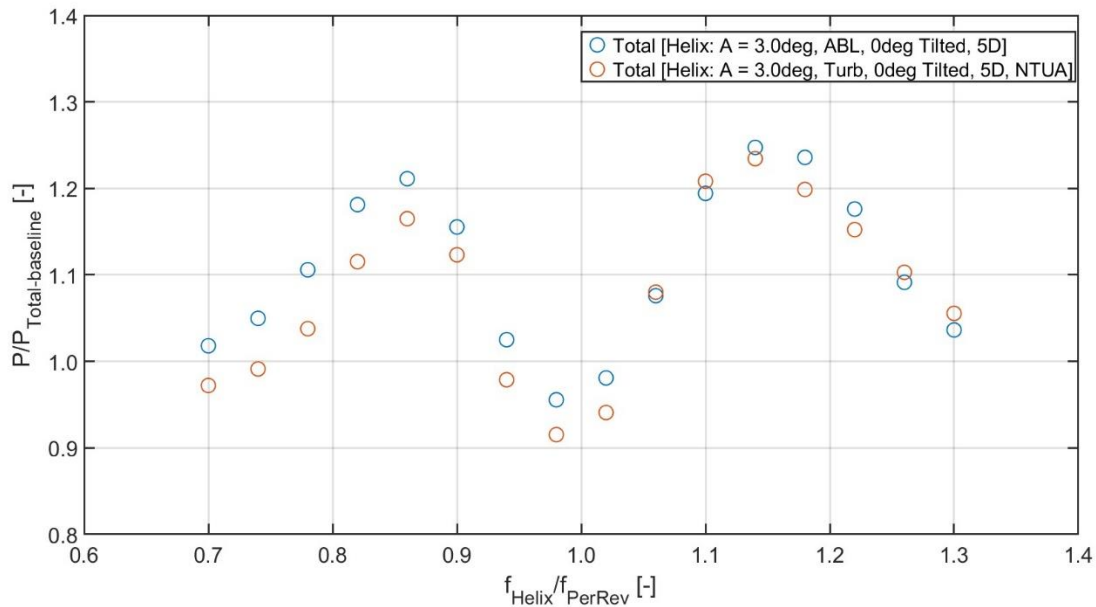


**Figure 34.** Relative power performance of the two turbines with respect to the no control case. NTUA: High Turbulence inflow, TUM: ABL inflow. Comparison between measurements at TUM and at NTUA.

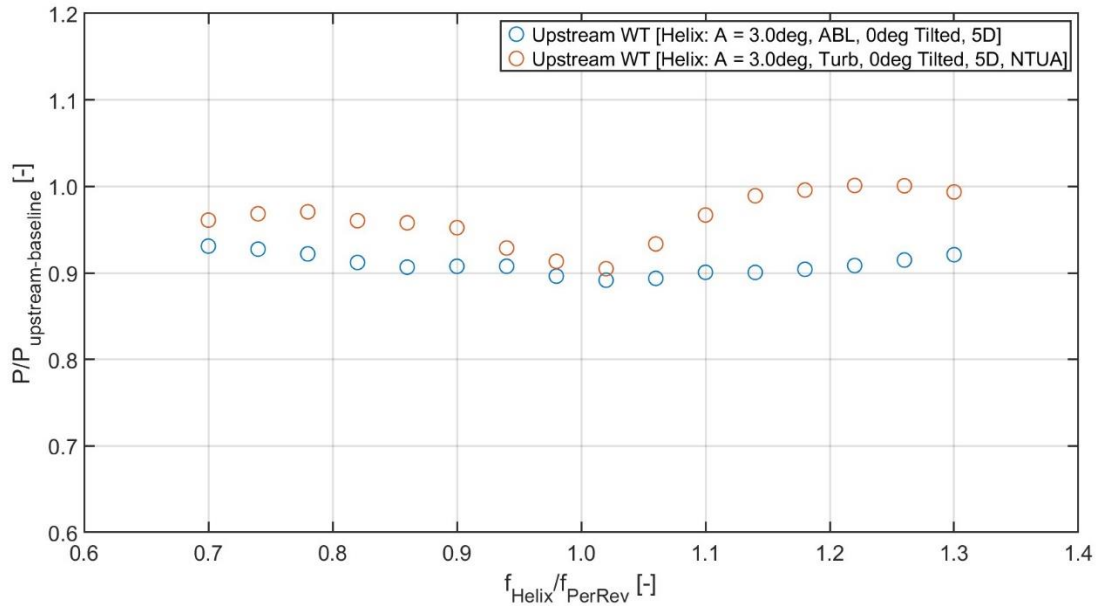


**Figure 35.** Relative power performance of the upstream turbine with respect to the no control case. NTUA: High Turbulence inflow, TUM: ABL inflow. Comparison between measurements at TUM and at NTUA.

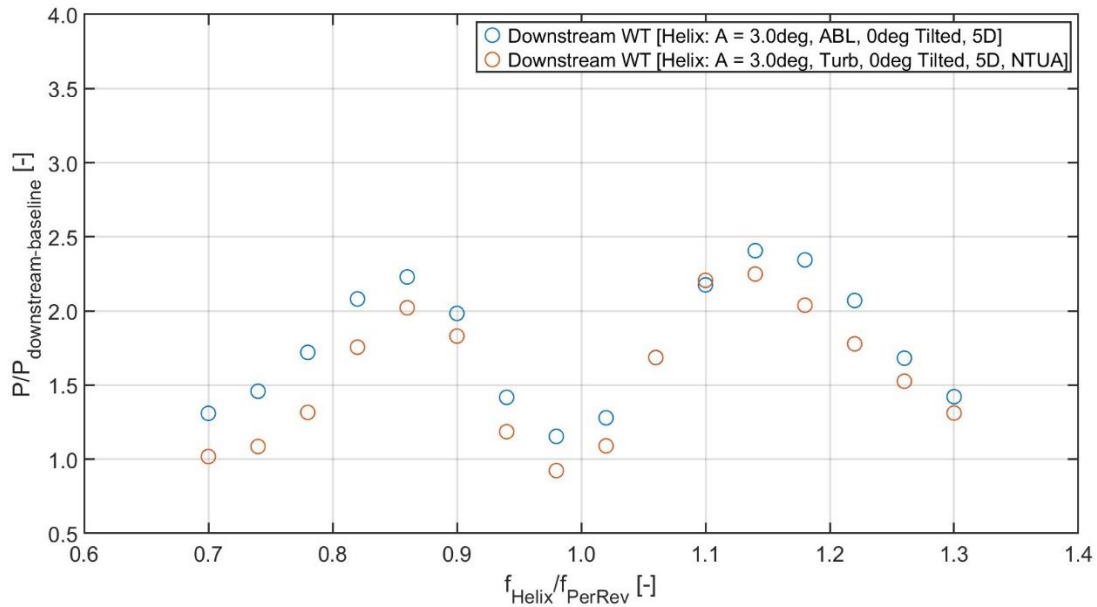


**Figure 36.** Relative power performance of the upstream turbine with respect to the no control case. NTUA: High Turbulence inflow, TUM: ABL inflow. Comparison between measurements at TUM and at NTUA.

#### 4.2.4 Combination of Helix with Static Yaw – Low Turbulence

To the best of the authors knowledge a combination of Helix and Static yaw combined control was first tested during this twin test. Preliminary results from both facilities, shown in Figure 37, Figure

38 and Figure 39 for the low turbulence inflow case, suggest that the combined control is not beneficial for the wind farm set up compared to a Helix only case.

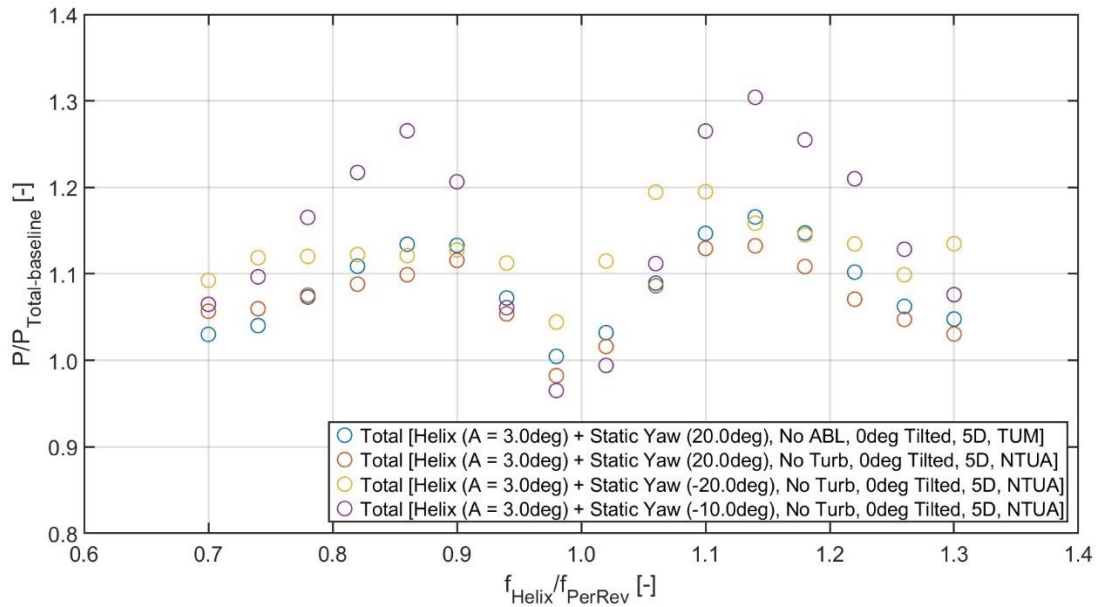


**Figure 37.** Relative power performance of the two turbines with respect to the no control case. Combination of Helix and Wake Steering (Static Yaw). Low turbulence inflow. Comparison between measurements at TUM and at NTUA.

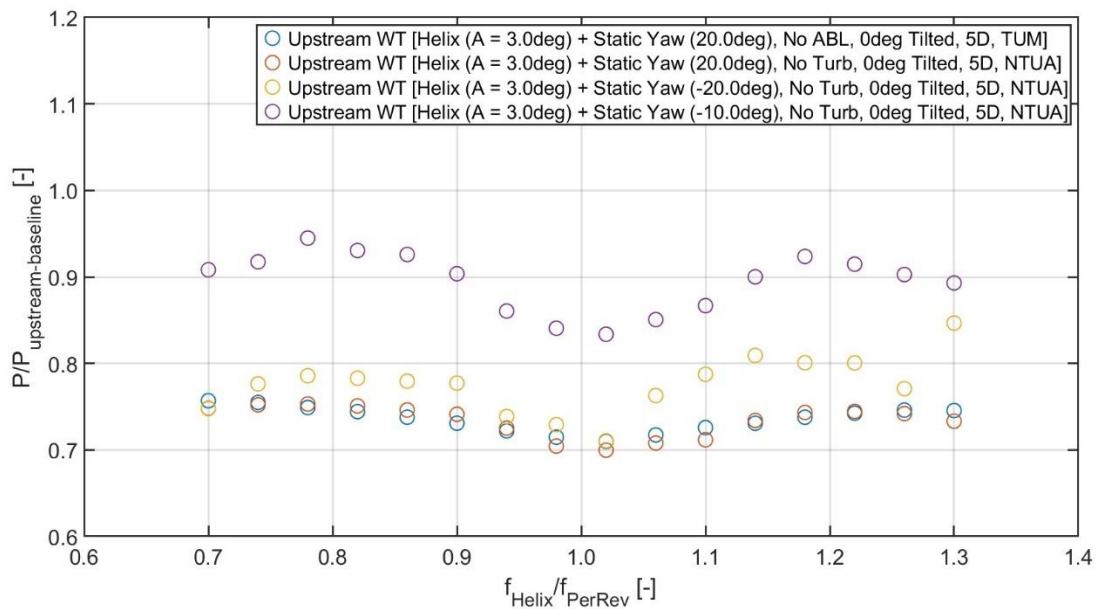


**Figure 38.** Relative power performance of the upstream turbine with respect to the no control case. Combination of Helix and Wake Steering (Static Yaw). Low turbulence inflow. Comparison between measurements at TUM and at NTUA.

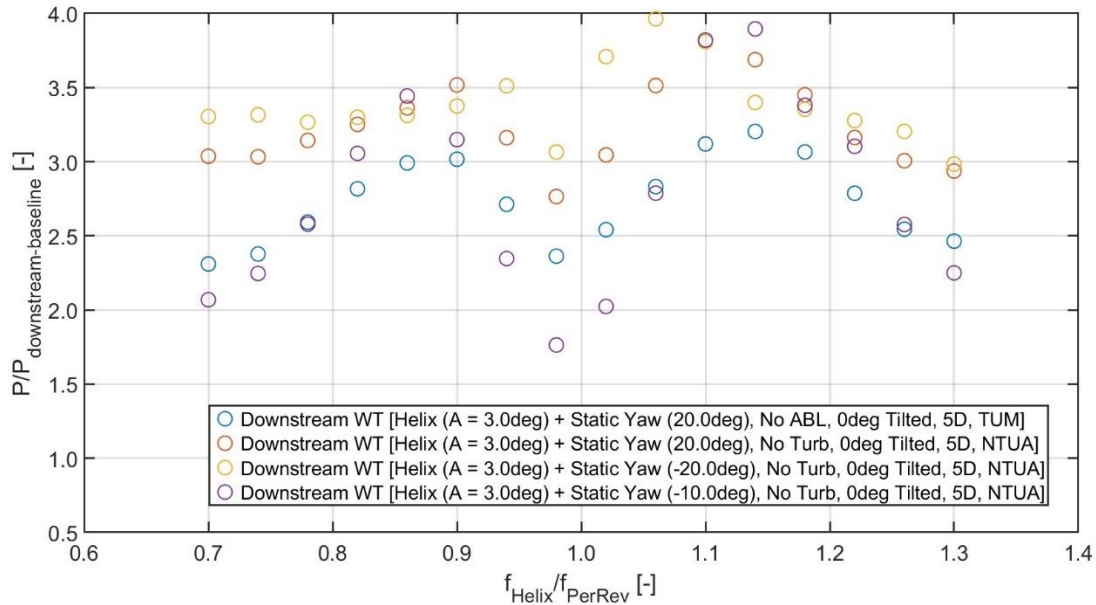


**Figure 39.** Relative power performance of the downstream turbine with respect to the no control case. Combination of Helix and Wake Steering (Static Yaw). Low turbulence inflow. Comparison between measurements at TUM and at NTUA.

#### 4.2.5 Combination of Helix with Static Yaw – High Turbulence

The good agreement between the results obtained at two different facilities also hold for the high turbulence case with the two wake control methods combined. Results shown in Figure 40, Figure 41 and Figure 42 again confirm that the combined affect of the two wake control methods is not beneficial.

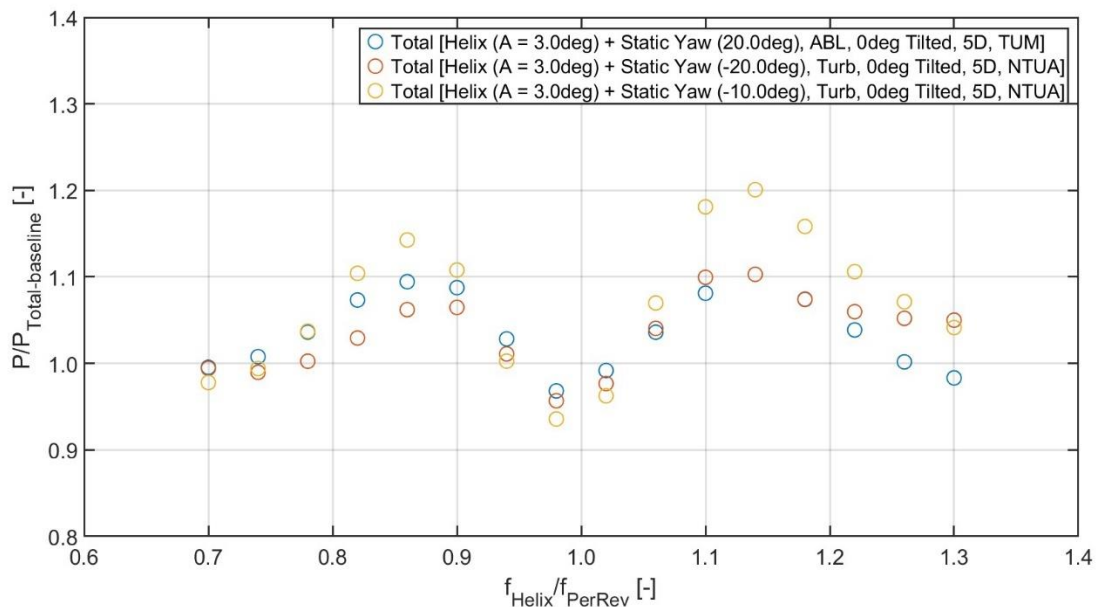


**Figure 40.** Relative power performance of the two turbines with respect to the no control case. Combination of Helix and Wake Steering (Static Yaw). High turbulence inflow. Comparison between measurements at TUM and at NTUA.

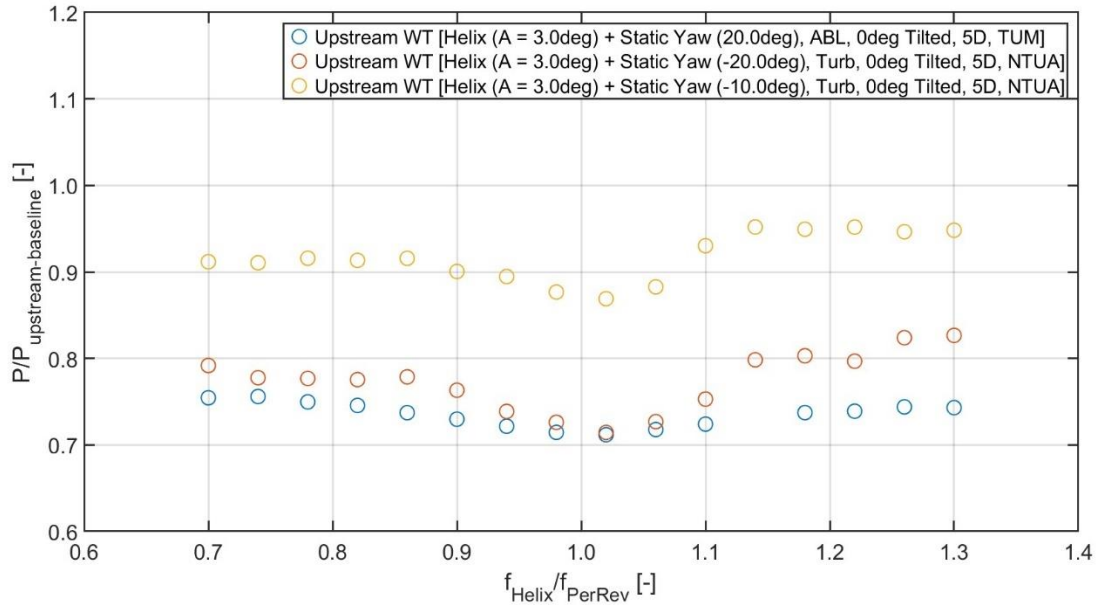


**Figure 41.** Relative power performance of the upstream turbine with respect to the no control case. Combination of Helix and Wake Steering (Static Yaw). High turbulence inflow. Comparison between measurements at TUM and at NTUA.

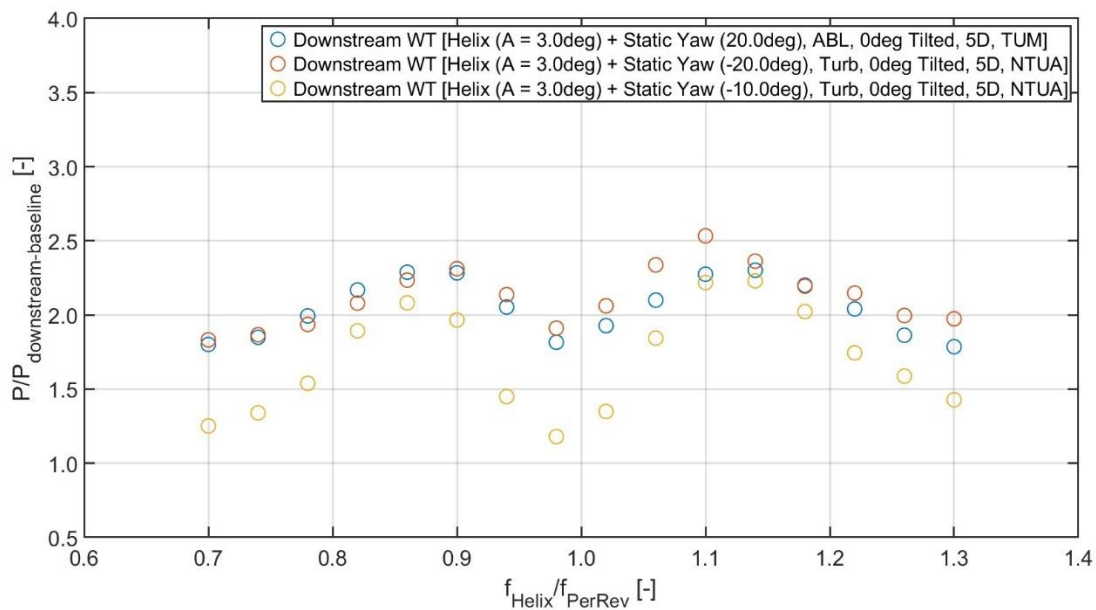


**Figure 42.** Relative power performance of the downstream turbine with respect to the no control case. Combination of Helix and Wake Steering (Static Yaw). High turbulence inflow. Comparison between measurements at TUM and at NTUA.

## 5 Conclusions

This chapter presented the facilities, equipment and set up details for the two campaigns performed at NTUA and TUM within the scope of Twin Test 2 of the TWEET-IE project. The experience gained was significant for everyone involved and, in addition, new data and knowledge were generated. The agreement between comparable set ups at the two wind tunnels is encouraging despite differences in the inflow turbulence profiles and blockage ratios. The effects and trends of the two tested wake control techniques are confirmed during two different campaigns and the results will lead to new publications. It is also noted that the baseline results (no wake control) form the basis of the TWEET-IE blind test<sup>1</sup>.

---

<sup>1</sup> [doi.org/10.5281/zenodo.10566400](https://doi.org/10.5281/zenodo.10566400)

## 6 References

- [1] Kozmar H 2011 Wind-tunnel simulations of the suburban ABL and comparison with international standards *Wind Struct. An Int. J.* **14** 15–34
- [2] Heckmeier F M 2022 Multi-Hole Probes for Unsteady Aerodynamics Analysis
- [3] Heckmeier F M and Breitsamter C 2020 Aerodynamic probe calibration using Gaussian process regression *Meas. Sci. Technol.* **31** 125301
- [4] Mühle F V, Heckmeier F M, Campagnolo F and Breitsamter C 2024 Wind tunnel investigations of an individual pitch control strategy for wind farm power optimization *Wind Energy Sci.* **9** 1251–71
- [5] Bottasso C L and Campagnolo F 2022 Wind tunnel testing of wind turbines and farms *Handb. Wind Energy Aerodyn.* 1077–126
- [6] Campagnolo F, Castellani F, Natili F, Astolfi D and Mühle F 2022 Wind Tunnel Testing of Yaw by Individual Pitch Control Applied to Wake Steering *Front. Energy Res.* **10** 883889
- [7] Campagnolo F, Petrović V, Schreiber J, Nanos E M, Croce A and Bottasso C L 2016 Wind tunnel testing of a closed-loop wake deflection controller for wind farm power maximization *J. Phys. Conf. Ser.* **753** 032006
- [8] Wieneke B 2008 Volume self-calibration for 3D particle image velocimetry *Exp. Fluids* **45** 549–56
- [9] Schanz D, Gesemann S, Schröder A, Wieneke B and Novara M 2012 Non-uniform optical transfer functions in particle imaging: calibration and application to tomographic reconstruction *Meas. Sci. Technol.* **24** 24009
- [10] Schanz D, Gesemann S and Schröder A 2016 Shake-The-Box: Lagrangian particle tracking at high particle image densities *Exp. Fluids* **57** 1–27
- [11] Hansen M O L 2008 *Aerodynamics of wind turbines* (Earthscan)
- [12] van der Hoek D, den Abbeele B Van, Simao Ferreira C and van Wingerden J 2024 Maximizing wind farm power output with the helix approach: Experimental validation and wake analysis using tomographic particle image velocimetry *Wind Energy* **27** 463–82

